

DIEstro
Motion sensor platform for cattle oestrus detection

Author: Bruno Bellini

Tutor: Alfredo Arnaud

Master of Science in Electrical Engineering
Department of Electrical Engineering
Faculty of Engineering and Technologies - Universidad Católica del Uruguay
Montevideo, Uruguay

December 16th 2016

Acknowledgements

Firstly I would like to thank the people who helped me out in this project: Alfredo Arnaud for being a great mentor and tutor in this project and in the rest of my professional life, to Julio Acuña, who is in charge of the electronics workshop in BQN, for helping me when the soldering became hard, Rafael Puyol for listening my ideas, problems, and solutions everyday while this project was executed, and to Jorge Barboza, Diego Ganduglia and Carlos Santana from CCC who selflessly helped me with soldering also.

I would also like to thank the company where I work, BQN, for trusting in me and my capacities, giving me the economic support for materials and equipment.

A big thank also to ANII (Agencia Nacional de Investigación e Innovación) for supporting this project with a student grant, and to Universidad Católica del Uruguay (UCU) for providing me the possibility of improving academically everyday.

And finally, to my beloved wife, who supported me on frustrating moments and always encouraging me to go ahead.

Abstract

The reproductive efficiency of dairy industry has decreased over the last ten years due mainly to an intensification of the management techniques of the herd, and an increase of the total number of animals. A main objective of worldwide dairy farms is to ensure that dairy cows, produce as much milk as possible. A cow produces milk while it has a calf to breastfeed, therefore, the less time passes between births, the more "productive" the cows are. This is the principal reason why the precise heat (oestrus) detection has become so important, a task traditionally assigned to veterinary and expert people examining and watching the cattle behaviour, and in recent years to electronic devices monitoring the cow's physical activity.

Tracking the animal's physical activity by means of a portable device strapped to each animal, is known to be a very effective way to determine heat, but sometimes requires expensive hardware and large batteries.

In this work, a low-cost micropower wireless system able to automatically detect oestrus period of cattle is presented. It was designed in cooperation with BQN, a company developing technology for the agribusiness industry in Uruguay. The tracker seizes the recent availability of 1 uA micropower accelerometers, LoRa long range transceivers, and FRAM microcontrollers, to achieve a coin cell battery powered paradigm for oestrus detection. The device records 3 axis acceleration information, process it, and periodically sends it to a server; it has a measured ultra low power consumption of 5 uA while collecting/processing data, reaching a very large ($> 10km$) communication distance using a star topology and LoRa technology at countryside areas.

The scope of the project and this documentation is the entire hardware and firmware development, from the start idea, design and final implementation.

Keywords: WSN (Wireless Sensor Network), LoRa (Long Range Communication), Low Power, Accelerometer, Motion Sensor, Heat Detection, Embedded System, FRAM, Cattle.

Contents

1	Introduction	5
1.1	Objective	5
1.2	Background	5
1.3	Specifications	6
1.4	Document organization	6
1.5	Theoretical framework	7
1.5.1	Oestrus detection importance	7
1.5.2	Oestrus detection with accelerometer methods	14
2	Proposed solution	18
2.1	Hardware	19
2.1.1	General Description	19
2.1.2	Accelerometer: ADXL362	20
2.1.3	LoRa: Long Range Communication, SX1276	22
2.1.4	Microcontroller: MSP430	31
2.1.5	Power Supply	33
2.1.6	Antenna	36
2.1.7	Layout design and PCB	37
2.2	Firmware	40
2.2.1	Code structure	41
2.2.2	Microcontroller Memory Layout	44
3	Tests and results	46
3.1	Power consumption	47
3.1.1	Practical measurement	47

3.1.2	Battery lifetime	50
3.2	LoRa communication	51
3.2.1	Data transmission time	51
3.2.2	Communication distance measurements	52
4	Conclusions	55
4.1	Improvement opportunities	58
4.2	Costs and Market	58
4.3	Publications	58
	Appendices	64
A	Schematic Circuit and BOM	65
B	FW Modules	69
C	Long Range Wireless Communication - LoRa	71
D	FRAM	80
E	BSL-Rocket and BSL-scripter	83
F	Previous work	86

Chapter 1

Introduction

1.1 Objective

The main goal of this project was to design and build an ultra low power motion sensor platform aimed at cattle oestrus detection. The final result should be a state of the art embedded system including an accelerometer and a low power but long range communication hardware, an embedded firmware implementing the data acquisition and basic algorithms for heat detection, all able to run a couple of years from a single small primary (non rechargeable) battery.

1.2 Background

BQN is a Uruguayan IT company, which develops and manufactures electronic equipment and software products, and also offers advisory, consulting and custom development in electronics. It has developed products in the area of POS (Point Of Sale), medical electronics and RFID technology applied to traceability within the agribusiness industry.

On September 2006, Uruguay, a country with four more times cattle than people, became on the first country to have a mandatory cattle traceability system. Nowadays 100% of the cows have a visual and an electronic tag, containing an unique identification number, attached to its ear, ensuring traceability from birth during the full life cycle of the animal.

BQN observed an opportunity to seize its experience in the development of portable electronics, and in 2010 launched *Baqueano*, its first RFID reader for the agribusiness industry, and since then more than 2000 readers have been commercialized in Uruguay, Chile, Paraguay and Colombia. This product is the best sold and still the only RFID reader produced in Uruguay in large quantities. At present, the idea is to expand the product range for the industry at BQN, including a farm-management web system, and an embedded system able to automatically detect heat of cattle mainly in the dairy farms. This second product is the topic of interest of this document.

In this work, a first prototype of a low-cost micropower wireless system, able to automatically detect oestrus period of cattle and transmit the information to a server a few kilometers away, is presented. The developed device may result valuable for the industry, but also has academic interest since it incorporates true state of the art electronics like 1 uA accelerometers, LoRa transceivers, and a FRAM microcontroller.

1.3 Specifications

The general specifications of the system were created at the very early stage of the project, and they were obtained from a survey of different existing commercial products on Internet, interviewing veterinaries, talking to current clients of the Baqueano RFID readers, and finally trying to imagine how the system would-should-could be used.

From all the gathered ideas, the strengths and weaknesses of existing products were detected and used to develop the specifications for a competitive product to later introduce in the market.

Behaviour

DIEstro is a motion sensor platform capable of registering processed acceleration data of a single cow, and then sending this data to a concentration server which implements the high-level intelligence to determine if there is oestrus present or not. Future work may involve to do the heat detection in the platform itself.

General specifications

A list of the initial specifications follows; the embedded system shall:

- Record information about acceleration data. Preferably three axis.
- Be able to record at least one hour of acceleration samples.
- Work correctly on a temperature range between 0°C and 50°C.
- Have a long range and simple wireless communication method to transmit data.
- Reach a very low power consumption profile. Take its power from a primary battery for at least 2 years.
- Be integrated in a rough case in order to withstand the harsh environment it will work into.
- Be placed on the cow's neck as a collar, with intention of upgrading it to an ear tag system.

1.4 Document organization

This document is divided into 4 chapters and 6 appendixes, where each one of them have a particular topic on the development of the project.

The rest of this chapter presents the theoretical framework, discussing existing products and techniques for cattle oestrus detection in the market, and recent research in the academic field.

Later, *Proposed solution* chapter presents the final implemented hardware and firmware. At *Hardware* section all the related aspects to the final hardware equipment are treated, each component and the selection criteria adopted in each case is described, while *Firmware* section presents the software architecture election for the MSP430FR microcontroller, code structure, implemented algorithms, etc.

Moreover, the *Tests and results* chapter is presented. As its name indicates, it shows in detail which were the measured characteristics of the system to determine the defined objectives accomplishment.

Main structure of the document is finished with *Conclusions* and *Bibliographic references*.

Finally, a series of *Appendixes* are presented where extra information about the project is presented.

1.5 Theoretical framework

1.5.1 Oestrus detection importance

The reproductive efficiency of dairy industry has decreased over the last ten years due mainly to an increasing individual production of the cows, an increase of the total number of animals and an intensification of the management techniques of the herd.[1] A poor percentage of correct heat detection is described by Senger[2] as the most important problem, limiting high reproductive efficiency.

One of the main objectives of worldwide dairy farms is to ensure that dairy cows produce much milk as possible. A cow produces milk while it has a calf to breastfeed, therefore, the less time passes between births, the more "productive" the cows are. In addition, as Vanrell states in his work [3] "successful artificial insemination relies on correct heat detection because it is only possible in a short-time window after heat". This is the main reason why the correct heat detection has become so important.

The reproductive efficiency of dairy cattle is commonly measured by the calving interval (CI), parameter which affects daily milk production (liters) of the cow during its life, and the income from sales of associated milk production. The CI is determined by the voluntary waiting period, the percentage of heat detection (PHD) and conception rate (CR). The cows in a herd will be pregnant (pregnancy rate, PR) after the voluntary waiting period depending on the PHD and CR:

$$PR = PHD \times CR \quad (1.1)$$

The PR represents the proportion of cows that become pregnant during each oestrus cycle and is directly linked to the number of days after the voluntary waiting period, required for cows to get pregnant. As the PR increases, due to greater PHD and/or CR, the CI decreases.[1]

At present, most operators of dairy farms have to visually detect, among the herd, which are those animals that are in heat. Once identified, they have to separate them out for insemination. Therefore, the PHD is determined by the intensity and accuracy (ability of the operator to recognize the clinical signs of oestrus) of heat detection. The CR is determined by the number of diagnosed pregnant animals on the number of inseminated ones. Achieving a 90% of PHD and 50% of CR, a 45% PR is obtained during a cycle of insemination of 21 days. If the CR is maintained constant and PHD decreases 50% (1 cow in 2 detected) the PR will decrease to 25%. This situation is quite common in medium and high dairy production in our country.[4]

It is generally accepted that the efficiency of heat detection is less than 50% in most dairy farms. To achieve an acceptable reproductive performance, it is required to do the *first service* on time and to quick identify the cows that are empty to serve them again. Errors in heat detection are a common problem of dairy farms and should always be considered as a cause of low conception rate. Improving the PHD by technologies as the one presented in this work, PR increases (CI decreases), thus increasing productivity.

To better visualize the problem, it is interesting to consider that worldwide between 20% and 50% of the heats are lost and more than 30% of cows are inseminated when they are not in heat.

Although many dairy cows well fed and healthy start to cycle about 3 weeks after birth, early heats are not very obvious. The intensity of heat increases with each passing day postpartum, resulting in an increase in heat detection rate when the postpartum interval is bigger.

According to Jonsson at [5] "conditions for identification of oestrus and successful artificial insemination have become more difficult in recent years due to reduced expression and decreased duration of oestrus".

The increase of heat detection has several positive impacts. The most important are: improved insemination results, controlled calving interval and total pregnancy rate. On the other hand, errors on heat detection (undetected or falsely detected) lead to unsuccessful inseminations (not in time or the animal not in heat) and therefore prolonged calving intervals. With these errors, farmers lose time, semen, and direct "losses of income due to unexploited potential of milk and calf production". At his work [6] Firk presents a study where daily losses are presented. Calculated costs are "of 0.63-1.25 Dollars per day of prolonged calving intervals. A decrease in conception rate of 1% results in costs of 1.62 Dollars per cow per year".

1.5.1.1 Bovine oestrus characteristics

Cows should cycle every 21 days, but more than 90 percent of the cows should show signs of heat for the day 50 postpartum. The most reliable sign of a cow in heat is the behaviour to allow mounting, which is the time when the animal allows to be mounted by another animal in the herd.

Cows are mounted, on average, 1.5 times per hour and every heat is visible for about 6-8 hours, although its full duration is approximately 12 hours. Firk affirms that depending on the breed, the oestrus period oscillates between 12-16 h with a mean duration of 13.5 h and a standard deviation of 2.3 h [6]. So that, cows are in heat a little more than a third of the day and only spend a total of 3 to 5 minutes mounting each others.[7]

According to Bosques-Mendez [7], some noticeable indicators of the presence of oestrus are:

1. Passivity when mounted is the strongest indicator that the cow is in heat. It consists of the immobility of the female for 5-8 seconds when mounted by the bull or another partner in the group.
2. During the Proestrus (period of time before oestrus) females sniff and lick the genitals of their companions.
3. The cows are restless, walk more often, moo, rub between them, leave their calf.
4. Cervical mucus more evident in heifers than in cows.
5. As a result of repeated mountings, rump area is shaved.
6. Vulvar edema due to estrogenic action.
7. Low milk production and poor appetite.

It should be pointed out that indicators 1, 2, 3 are reflected in the physical activity of the animal, thus an accelerometer can be used to track these symptoms and guess oestrus with a high likelihood

degree. But the animal's activity as indicated in 3 is by far the easiest and the most accurate method to determine heat.

Bosques-Mendez asserts that the highest conception rate (CR) occurs if the animals are inseminated within 4-14 h after the onset of oestrus. With a good heat detection, time of insemination should follow the AM-PM rule. An animal in heat in the morning (AM) should be inseminated in the afternoon (PM). An animal observed in heat in the afternoon (PM) should be seeded in the early hours of the next morning (AM). With a better heat detection percentage it is expected to have also a better conception rate.

1.5.1.2 Oestrus detection methods

Different methods have been employed for oestrus detection in farms, some of them are:

- Visual Oestrus Detection
- Technical Systems
 - ◊ Progesterone Test
 - ◊ Milk Yield
 - ◊ Body and Milk Temperature
 - ◊ Vaginal Mucus Resistance
 - ◊ Mounting Activity
 - ◊ Walking Activity

Visual Oestrus Detection

According to Bosques-Mendez, three or more observations of 20 minutes each, early morning, noon, and evening, are necessary to detect more than 60 percent of the cows in heat.[7]. In addition, Roth (as cited in Firk's work) "considered five observation periods of 20-30 minutes as essential for effective oestrus detection, but emphasized that these observation frequencies are not realizable on commercial dairy farms".[6]

The partner cows play a significant role in heat detection program. Pregnant cows, or those found in the early luteal phase of her oestrus cycle are not good sensing heat. Cows in heat, getting into, or out of heat are excellent detectors. By increasing the number of cows in heat, the number of mounts per episode of visible heat also increases.

It is important that rodeos have sufficient cycling animals and at least one animal entering oestrus each day. This requires a minimum of 21 cycling cows in the herd at all times. Cows tend to congregate in certain areas when they are in heat.

Routine visual method has a low PHD (between only 50% and 60% of cows in heat are correctly detected) and demands long working hours of the farmers against any climatic condition.[1]

According to [6], "efficient oestrus detection by visual observation is time-consuming and requires diligent attention". Geers (as cited as Firk's work) specified that from the total labour time in commercial farming, heat detection requires a 30%. Also, Firk presents different studies where Williamson detected 56% of oestrus by visual observation, Liu and Spahr reported a detection rate of

58%, and At-Taras and Spahr detected 54.4%-54.7% of oestrus by visual oestrus detection. Having a good automatic heat detection method not only improves PHD, but also saves time to farmers.

Technical Systems [6]

In order to improve visual detection results, it is natural to think of using technology to improve results and save costs. Nowadays, there are several technical methods for heat detection based on different principles: chemical, physical, and behavioral.

As it is presented in Firk's work, an optimal heat detection system should provide continuous monitor of the animals, individual identification, operation for the productive lifetime of the cow, high accuracy in identifying the appropriate physiologic or behavioural events that correlate with ovulation, and all of them with minimal labour requirements for the farmers.

Progesterone Test

When a cow is in heat, there is a notorious change in progesterone content in blood or milk. Although progesterone content measurement is easier to perform in milk samples, the result highly depend on the level of milk fat.

Disadvantages of this method are:

- Changes in progesterone levels do not occur at first oestrus after calving.
- Relatively high costs.
- Not practical for the farmer.

Milk Yield

Firk's work [6] presents several studies related to milk yield when cows are in heat. While some of the cited authors by Firk affirm that significant changes in milk yield were found, on the other hand there are authors that asseverate that the milk yield change could not be directly related to the heat period. According to the promoters of this method, decreases of milk yield between 2%-8.2% were reported on the day of oestrus for cows housed in free stall barns. However, detractors explain that lower milk production during oestrus could be associated with increased restlessness and decreased feed intake, or the day of lactation, and then they doubted that a decline of milk yield has sufficient magnitude or precision to replace other oestrus detection methods.

Body and Milk Temperature

The normal body temperature of a cow is approximately approximately 38.6 °C, but during the heat cycle significant changes in body temperature may occur. These changes are explained at Firk's work as:

- Before heat temperature decreases. The minimum temperature is reached 2 days before oestrus.
- When in heat, temperature rises between 0.1 °C and 0.5 °C.

However "an increase of body temperature is not a specific indicator for incidence of oestrus. Systemic and local inflammatory reactions might also cause increased body temperatures." [6]

Measurements of temperature can be performed directly via the rectum, by implants or indirectly in milk. These measurement methods are time-consuming and not practicable on commercial dairy farms.

Vaginal Mucus Resistance

Hormonal changes effect the electrical resistance of vaginal mucus during oestrus cycle. A minimum of vaginal mucus resistance is reached 25 h before ovulation. However, resistance of vaginal mucus is highly influenced by several non-oestrus related parameters and therefore is unsuited to oestrus detection. Practical application is complicated because of difficult, time-consuming manual measurements with the risk of inflammation.[6]

Mounting Activity

Several technological aids exist for registration of successful mountings. One possibility is the application of a video recorder. Disadvantages of this system include problems with the correct identification of cows in oestrus, and the fact that application is only possible when the cows are held in free stall barns.

In support of visual oestrus detection, mount detectors were developed. Mount detectors are attached to the cow's rump and are indicated as an effective oestrus detection aid with the advantages of being easy to apply, easy to use and requiring little time and labour. Different mounting activity methods are used: coloured lightchanging mount detectors, marking cows tail base with paint before they are in oestrus, the use of androgenised steers or surgically altered bull, to detect oestrus.

Walking, Standing, Lying Activity

As the bigger is the time the cows are visually observed, the more accurate the heat detection is, it is natural to think of an automated method which can monitor the cows behaviour the most of the time as possible.

An important external indicator for incidence of oestrus is restlessness. On the heat day the cows present higher activity rates than on previous days. At Firk's work some study cases are presented, where increased activities of up to 400% were found by in 93% of oestrus periods, with significantly higher locomotion rates in the afternoon and evening compared to the morning, and pointing out that each cow forms her individual activity process with different levels of increase for successive oestrus. The social rank of a cow in the herd influences sustainable activity behaviour.

Obvious differences in percentage increase of activity in oestrus are found between cows kept in free stall barns (93%) and tied stalls (14%-20%).

Deviations in activity during oestrus are detectable by comparing the activity value of the day of oestrus with activity values of a reference period. Possible reference periods are the dioestrus of the same cow, the previous day, the dioestrus of all cows and the whole oestrus period of all cows.

Detection of oestrus can be performed by utilization of different threshold values. For example, increases of the mean value by one or two standard deviations. Other possibilities for oestrus detection are exceeding a scaled value or using a confidence interval. Most common are thresholds of relative increases compared to earlier measurements, and it is what is intended to do in this work as explained further.

1.5.1.3 Criteria for evaluation of traits and methods

The performance of a detection system can be described as combinations of true and false responses. Oestrus that were correctly detected are assigned the status true positive (TP). Non-detected oestrus are rated as false negative (FN). Observations outside an oestrus period are true negative (TN) if there is no alert, otherwise the status of observation is false positive (FP). Criteria for distinguishing accurately between oestrus and dioestrus are compiled in Table 1.1.

Criteria	Formula
Detection rate, detected heats, diagnosis rate, sensitivity, efficiency, detectability	$TP/(TP+FN)*100$
Specificity	$TN/(TN+FP)*100$
Error rate, rate of false positive responses, false rate	$FP/(TP+FP)*100$
Accuracy, predicting value positive	$TP/(TP+FP)*100$
Predicting value negative	$TN/(TN+FN)*100$

Table 1.1: Criteria for evaluation of traits and methods.

1.5.1.4 Method for analyzing time series

According to Firk et al. [6], the most effective method for analyzing serial data and making forecasts is time series analysis. Time series methods can be distinguished by the amount of simultaneously analyzed traits in univariate and multivariate methods. Commonly utilized time series methods for univariate analyzing are smoothed variance, day to day comparison, moving average and exponential smoothing. The basis for all oestrus detection methods and all traits is comparison of the actual observation value with a defined number of previous observations. If the deviation between both values exceeds a given threshold, which could be the standard deviation or a relative deviation, an oestrus alert is given.

- Univariate methods
 - ◊ Smoothed variance
 - ◊ Day to day comparison
 - ◊ Moving average
 - ◊ Exponential smoothing
- Multivariate methods
 - ◊ Fuzzy logic
 - ◊ Kalman filter
- Combination of parameters

Univariate methods for time series analysis

Smoothed variance

Smoothed variance for oestrus detection could be performed. For example, at Firk's work [6] a case is presented where the locomotion frequency in successive 12-h periods was recorded for calculation

of variances between diurnal and nocturnal differences. Successive variances were smoothed to obtain the smoothed variance. The smoothed root mean square variance, calculated by averaging the root mean square variance with the previous estimate of averaged root mean square variance, is used as base for oestrus detection.

Day to day comparison

Day to day comparison for oestrus detection could be performed. The current measurement (movement, temperature, milking, etc.) is compared with the previous measurement. If the relative difference between both values exceeds a given threshold, the cow is regarded as in oestrus.

Moving average

This method compares the cow's actual observation with a moving average of a defined number of previous observations of the same cow. Conditions for estimations by the mean are that the data must be stationary and randomly distributed. This method leads to better results than day to day comparison but requires more computing power, being data processing more suitable on the server side, and it is what will be implemented in this work.

$$\hat{Y}_{N+1} = \sum_{t=1}^N \frac{Y_t}{N} \quad (1.2)$$

Exponential smoothing

The method of exponential smoothing includes the advantages of moving averages, but additionally different weight can be given to previous observations. In many cases recent observations contain more information than older ones about what will happen in the future.

$$\hat{Y}_{N+1} = \sum_{t=0}^N \alpha * (1 - \alpha)^t * Y_{N-t} \quad \text{where } 0 < \alpha < 1 \quad (1.3)$$

The chosen alpha value decreases exponentially with increasing distance between history value and actual observation. A problem of the exponential smoothing method is the finding of the best value for α in such a way as to minimize the mean square error. The minimum mean square error must be determined through trial and error.

Multivariate methods for time series analysis

Multi-factorial analysis is becoming feasible, in which several information technology applications are implemented at the same time to support detection of oestrus, clinical mastitis and sub-clinical mastitis. Multivariate oestrus and mastitis detection were performed with fuzzy logic and with a Kalman filter.

Fuzzy logic

Fuzzy logic is a well known method applied in control, classification and decision support systems. The strategy of fuzzy logic systems is to tolerate a certain amount of missing precision, vagueness and uncertainty in the process of modeling. The specific use of this imperfect information implies a reduction of complexity in comparison to other systems.

Kalman filter

Processing of large amounts of data, such as production data in dairy herds, requires considerable computing time and storage capacity. These requirements can be solved by recursive calculation methods. In place of data, parameters of previous calculations are saved for further estimations. The Kalman filter is a recursive procedure with two stages which has initially been applied to problems of prediction and estimation of time series. A Kalman filter can be used for univariate and multivariate processing of data. The recursive estimation procedure of the Kalman filter is based on the state space formulation of a linear model. Kalman filter is suitable for serial analysis of temperature, activity, weight and food consumption measurements.

Combination of parameters

High amounts of false positive oestrus alerts is a consequence of exclusive consideration of single parameters. The required effort for supplementary manual examination would exceed a reasonable dimension. A combination of computer-based management functions with operating assignments for computer-based sensor technique in a superior herd management program could improve results. As a result, a reduction of costs in comparison to single systems is expected and breeding and selection decisions could be justified economically.

1.5.2 Oestrus detection with accelerometer methods

There are several studies and publications referring to the study of cows behaviour and oestrus detection from activity measurement, implemented by a 3-D accelerometer and wireless communication [8][9][10][11][12]. Most of them implement different techniques, methods, and algorithms to identify cows behaviour, and hence, reproductive state.

1.5.2.1 Classification

Bikker at [13] evaluated a 3-dimensional accelerometer device from Agis Automatisering, which can be attached to ear identification tags. Based on the principle that behaviour can be identified by ear movements, a proprietary model classifies sensor data as *ruminating*, *eating*, *resting*, or *active*. The authors compared accuracy and precision of the sensor method, against visual observation of 2 trained observers. Each minute of sensor and visual observation data was classified into 1 to 9 categories (8 behaviours and 1 transition behaviour) and summarized into 4 behavioural groups, which were analyzed by calculating kappa (k) values.

The CowManager SensOor is a product developed by Agis Automatisering. It comprises a moulded chip that can be connected to an electronic eartag of a cow for monitoring cow welfare. The CowManager system contains 4 modules: Fertility, Health, Nutrition and Find my Cow. The SensOor



Figure 1.1: CowManager SensOor device.

gives information about the herd, saves labour and ensures a sustainable herd [14]. A 3-dimensional accelerometer continuously registers the movements of the cow's ear. Data are sent through a wireless connection, via routers and coordinators, to a computer. The data logger allows data storage for a maximum of 48 h after the last communication. Raw data is continuously collected and each minute is classified as 1 of 4 behavioural categories, which are subsequently expressed as percentage of behaviour per hour as well as per day and are available through a web-based application.[13]

The CowManager system offers:[14]

- Oestrus detection.
- Precise timing of insemination.
- Detection of disease outbreaks.
- Continuous monitoring of the herd.
- Continuous measuring of rumination behaviour.
- Find cows with the *find my cow* application for Android smartphones.

The dataset, for this study, consists of measurements of steps and lying/standing behaviour recorded by the commercially available activity monitor IceTag3D. The sensor is attached to the dairy cows leg and assess the dairy cows activity in terms of the variables *lying*, *standing*, *motion index* and *step count* using 3d-accelerometer technology. The sample period of the IceTag3D is configurable and is chosen as 1 min.

The first three variables available from the IceTag3D are the percentage of the sample period spent in each of the three states. The fourth variable, the step count, is the number of steps in each sample period.



Figure 1.2: IceTag3D device.

IceTag3D features:

- 60-day memory
- Data can be viewed and manipulated down to individual seconds
- Data downloaded manually via desktop reader connected to PC

Vanrell at [3] proposed an oestrus detection method, where a recording device (collar) is attached to the cow, and acceleration records are filtered and segmented. After that, simple statistical attributes are extracted from each segment. Extracted features from a segment are put into a classifier, which decides if the record belongs to a normal cow or a cow in heat. Tested classifiers are multilayer perceptrons, support vector machines and decision trees.

The authors affirm that visual differences are not evident when signals recorded on normal cows and cows in heat are compared. Thus, a threshold, or some other rule, can not be defined. So that, a pattern recognition approach where the proposed system learns from labeled examples is applied. The feature extraction stage involves the conversion of the raw signal into a vector of attributes. In the classification stage, these feature vectors are given as an input to the classifier, which estimates the class that each vector belongs to.

A common strategy in the field of signal processing involves the division of the original records into time fixed-length segments and then the translation of each segment into a feature vector. Each feature vector x_i represents a segment labeled as i and is integrated by attributes extracted from a_x , a_y , a_z and $|a|$. Five attributes are extracted from the acceleration signal in each direction, which finally are organized to form a feature vector x_i of twenty elements. The features extracted from a high-pass filtered signal are five: energy, maximum, minimum, amplitude and standard deviation. This feature extraction process is developed using Matlab. The classification later is done by the software Weka using the following classifiers: Multilayer Perceptron (MLP), Support vector machines (SVM), and Decision trees (DT).

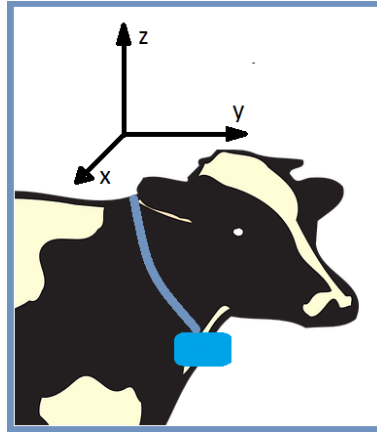


Figure 1.3: Schematic illustration of recording device attached to the top of the collar.

On [16], Dutta presents a system composed of a 3-axis accelerometer, a 915 MHz radio transceiver, and multi-classifier pattern recognition technique in order to classify cattle behavioural patterns.

In this chapter, an introduction to the cattle's heat characteristics, detection importance, and different methods for heat detection were presented. In the following chapter, a automated solution for heat detection using a 3-axis accelerometer and long range wireless communications is presented.

Chapter 2

Proposed solution

The approaches and solutions presented in the previous chapter for the oestrus detection problem are developed using different data analysis and processing methods, communication protocols, and network topologies. Figure 2.1 shows the proposed solution, where each cow has a collar, which includes a 3D accelerometer, a microcontroller, and a wireless transceiver, connected to a gateway. Meanwhile, the gateway is connected to Internet and sends the information to a server with a software application where data is processed and analyzed.

As one of the main goals of this project is to procure a simple, low power solution, but with long range communication distances, LoRa technology was selected to meet these requisites. LoRa (Long Range) technology [32] was introduced in 2013 by Semtech, and as explained in Appendix C, allows a long range communication in a star network topology, supporting up to ten thousand nodes connected to only one single gateway, at very low power consumption.

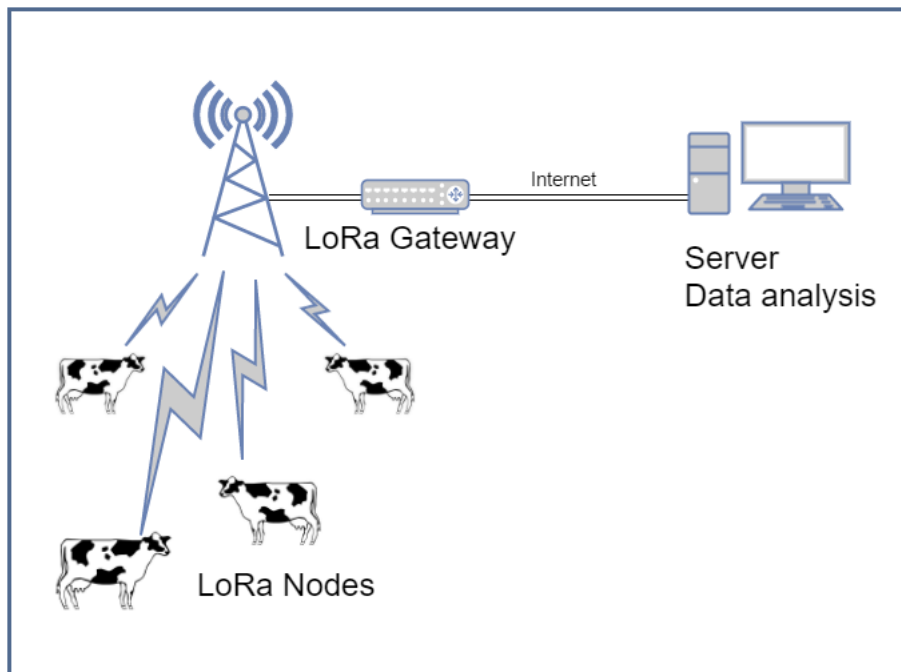


Figure 2.1: Proposed system solution.

2.1 Hardware

In this section, a deep hardware analysis is presented, starting with a general block diagram, then all the hardware components are presented and finally, each stage of the circuit is explained.

2.1.1 General Description

The hardware developed has its focus on the system low power nodes described previously. Each node is installed in a collar for cattle and measures the animal's motion activity and to do so, a low-power accelerometer is used. 3-axis acceleration samples are taken at 25 Hz, stored and processed each 6 seconds. Cow's activity was estimated of movements from 0.5 Hz to 7 Hz, therefore the acceleration samples are low-pass filtered by the accelerometer itself at half the bandwidth (12.5 Hz) and high-pass filtered by software to remove the mean value of each axis avoiding offset values due to gravity. After that, a mean value of the modulus of acceleration vector is stored, and the process is repeated for a complete hour, where data is processed again to obtain a mean value per hour.

Mean values obtained per hour are used to characterize the animal's behaviour on previous days to the heat, and then a threshold is established. When the cow enters to its heat period, activity will increase and hour-to-hour comparison will trigger an alert when threshold is exceeded. Every mean value per hour is transmitted to the server where calculations are done.

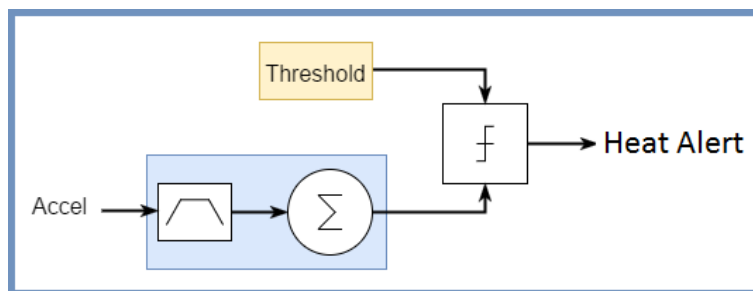


Figure 2.2: Heat alert logic implemented on the nodes.

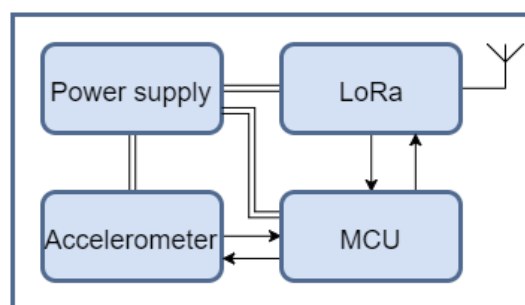


Figure 2.3: Block diagram of DIEstro hardware.

A brief discussion about different hardware elements (shown in Figure 2.3) follows, including:

- Accelerometer.
- Wireless communication: LoRa.
- MCU: MSP430.

- Power supply.
- Antenna
- Layout design.

2.1.2 Accelerometer: ADXL362

In order to measure the physical activity of cattle, a 3-axis accelerometer was employed. Particularly, the ADXL362 has an outstanding current consumption, which makes it ideal for battery powered devices.

	ADXL362	LIS3DHTR [34]	FXLN83xxQ [35]
Normal mode (ODR 50 Hz)	$1.8\mu A$	$11\mu A$	$182\mu A$
Normal mode (ODR 1 Hz)	.	$2\mu A$.
Shutdown supply current	$10nA$	$500nA$	$30nA$

Table 2.1: Current consumption comparison for different evaluated 3-axis accelerometers. ADXL362 is the accelerometer with the lowest current consumption in the market.

The ADXL362 is an ultra low power, 3-axis MEMS accelerometer, which consumes less than $2\mu A$ at a 100 Hz output data rate and 270 nA when in motion triggered wake-up mode. It provides a full bandwidth sample at all data rates and a configurable anti-aliasing filter at half and quarter of the output data rate (ODR).

The ADXL362 samples the acceleration vector as a 3 axis (x, y, z) value, and also samples temperature using its built-in micro-power temperature sensor. It provides 12-bit output resolution but a 8-bit formatted data is also provided when a lower resolution is sufficient, improving data transfer efficiency. Measurement ranges of ± 2 g, ± 4 g, and ± 8 g are available, with a resolution of 1 mg/LSB on the ± 2 g range. For applications that require lower noise levels than the normal $550\mu g/\sqrt{Hz}$, there are two other lower noise modes (down to $175\mu g/\sqrt{Hz}$ typical) that can be selected but leading to an increase in supply current.

In addition to its ultra low power consumption, the ADXL362 provides other features that can be used to reach a noticeable power reduction. It includes a deep multi-mode output FIFO, and several activity detection modes including adjustable threshold sleep and wake-up operation that can run as low as 270 nA at a 6 Hz (approximate) measurement rate. A dedicated output pin is provided to directly control, and it has provisions for external control of sampling time and/or an external clock.

The ADXL362 operates on a 1.6 V to 3.5 V supply range and is available in a 3 mm x 3.25 mm x 1.06 mm package.[36]

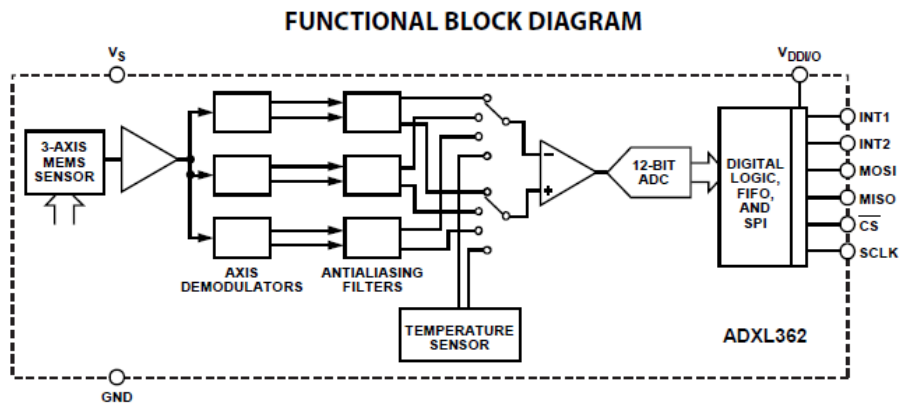


Figure 2.4: ADXL362 accelerometer functional block diagram (extracted from ADXL362 datasheet [36]).

2.1.2.1 Pinout description

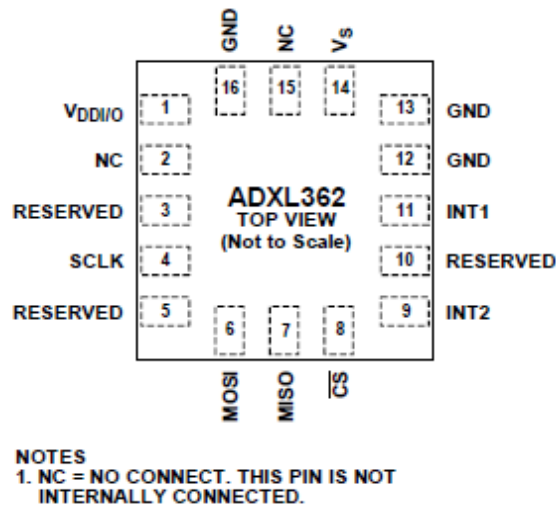


Figure 2.5: ADXL362 pin configuration (top view) [36].

In table 2.2 a description of functionality of each pin could be observed.

Pin No.	Mnemonic	Description
1	V_{DD}	Supply Voltage for Digital IO
2	NC	No Connect. Not internally connected
3	Reserved	Reserved. Can be left unconnected or connected to GND
4	SCLK	SPI Communications Clock
5	Reserved	Reserved. Can be left unconnected or connected to GND
6	MOSI	Master Output, Slave Input. SPI serial data input
7	MISO	Master Input, Slave Output. SPI serial data output
8	CS	SPI Chip Select, Active Low. Must be low during SPI communications
9	INT2	Interrupt 2 Output. INT2 also serves as an input for synchronized sampling
10	Reserved	Reserved. Can be left unconnected or connected to GND
11	INT1	Interrupt 1 Output. INT1 also serves as an input for external clocking
12	GND	Ground. This pin must be grounded
13	GND	Ground. This pin must be grounded
14	V_S	Supply Voltage
15	NC	No Connect. Not internally connected
16	GND	Ground. This pin must be grounded

Table 2.2: ADXL362 pin functions description [36].

2.1.3 LoRa: Long Range Communication, SX1276

One of the main goals of this project is to procure a simple, low power solution, covering big distances between nodes and data collectors (as it is intended to use on the countryside), and in order to meet these requisites LoRa technology was selected.

LoRa technology, promises great communication distances: around 2 km in city environments and 16 km on countryside. This wireless RF technology was created by Semtech [32], and is developed to create low-power, wide-area networks (LPWANs) required for Internet of Things (IoT) applications. The technology offers a mix of long range, low power consumption and secure data transmission and is gaining significant traction in IoT networks being deployed by wireless network operators.



Figure 2.6: LoRa gateway example.[32]

Some of the key features of LoRa technology are listed below [32]:

- **Long Range:** Deep penetration in dense urban environments (up to 2 km), and distances up to 20 kilometers between sensors and a gateway in rural areas.
- **Low Power:** The LoRaWAN protocol was designed for low power application thus enabling multi-year battery lifetime.
- **Geolocation:** Semtech asserts that tracking applications without GPS or additional power consumption can be done.
- **Standardized:** LoRaWAN ensures interoperability among applications, IoT solution providers and telecom operators. LoRaWAN specification standard was created on 2015.
- **High Capacity:** Supports 10000 nodes connected to a single gateway.
- **Secure:** Embedded end-to-end AES128 encryption of data.

2.1.3.1 LoRa and LoRaWAN introduction [37]

The main advantage of LoRa is in the technology's long range capability at a low power consumption. This kind of networks are known as *Low Power Wide Area Networks* (LPWAN) and were designed for wireless sensor applications that need to send small amounts of data, over long distances, a limited amount of times per day. LPWAN offers multi-year battery lifetime. In LoRa network, a single gateway can cover hundreds of square kilometers depending on the environment or obstructions in a given location.

Table 2.3 compares LPWAN networks with LAN and Cellular Networks. WiFi and Bluetooth technologies are widely adopted standards which have high data throughput, but they have short range coverage and poor battery lifetime. Cellular technologies are also well adopted with high data throughput and long range coverage, but poor battery lifetime and high costs.

	LAN	LPWAN	Cellular
Application	Short Range Communication devices	Long Range w/Bat IoT	Long Range w/Power Traditional M2M
Examples	Bluetooth, WiFi	LoRa, Sigfox	GSM, 3G, LTE
Standards	Well established	Emerging PHY solutions	Well established
Good for	Mobile devices In-home Short range	Long range Long battery Low cost Positioning	Long range High data rate Coverage
Not good for	Battery life Long range	High data rate	Battery life Cost

Table 2.3: Wireless standards comparison: Share of Market (SOM), advantages and disadvantages.[37]

LoRaWAN

LoRa technology is divided into two parts: LoRa physical layer and LoRaWAN. LoRaWAN is a standard that defines the communication protocol and network's system architecture while the LoRa physical layer enables the long-range communication link. LoRaWAN has the biggest impact in determining the battery lifetime of a node, the network capacity, the quality of service, the security, and the variety of applications served by the network.

To reach better communication distance ranges LoRa technology uses a **spread spectrum modulation** scheme that uses wideband linear frequency modulated pulses whose frequency increases or decreases over a certain amount of time to encode information. The main advantages of this approach are two: a substantial increase in receiver sensitivity due to the processing gain of the spread spectrum technique and a high tolerance to frequency misalignment between receiver and transmitter.

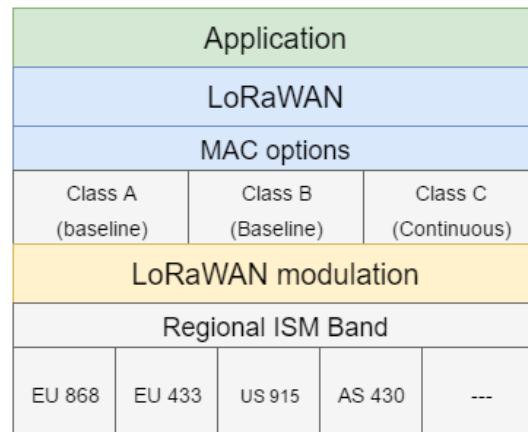


Figure 2.7: LoRaWAN stack layers.[37]

Network architecture

In order to reach a bigger communication range, "many existing deployed networks utilize a mesh network architecture. In a mesh network, the individual end-nodes forward the information of other nodes to increase the communication range and cell size of the network." [37] This type of networks have some disadvantages as adding complexity to the design and development, reduces network capacity, and reduces battery lifetime as nodes have to be "awake" to receive and forward information from other nodes irrelevant for them most of the time. On the contrary, a long range star architecture preserves battery lifetime, simplify network architecture, while long-range connectivity can be achieved.

In a LoRaWAN network nodes are connected to one or more gateways but they are not associated with a specific one. Consequently, data transmitted by one node is typically received by multiple gateways. Each gateway forwards every received packet from the end-node to a cloud server via Internet (cellular, Ethernet, Wi-Fi, etc).

The network server is in charge of managing the network. It solves redundant received packets, performs adaptive data rates, performs security checks. etc.

Battery lifetime

In order to reach long battery lifetime, LoRa nodes implement the Aloha method. Aloha method refers to a simple communications scheme in which each transmitter in a network sends data whenever it has to. If the packet successfully reaches the receiver, the next packet is sent when needed. If the packet fails to be received at the destination, it is sent again. Hence, "the nodes in a LoRaWAN network are asynchronous and communicate when they have data ready to send whether event-driven or scheduled" [37]. This is a big difference from mesh networks or with a synchronous networks, as the nodes periodically have to "wake up" to synchronize with the network. This synchronization scheme leads to significant energy consumption and thus of battery lifetime reduction.

Network capacity

Long range star networks are based on the possibility of their gateways to receive messages from a high number of nodes. This high network capacity is achieved by LoRaWAN networks by using multichannel multi-modem transceivers in the gateways and adaptive data rate. Capacity is affected by different factors, as the data rate, payload length, the number of concurrent channels or time between transmissions from the nodes.

LoRa physical layer is a spread spectrum-based modulation, so that, when different spreading factors are utilized, the signals are orthogonal to each other, different data rates are applied, and different transmission times (Time On Air) coexist. Based on these properties, the gateways are able to receive packets from multiple nodes on the same channel at the same time.

LoRaWAN utilizes an adaptive data rate to optimize the battery lifetime of nodes. It is reasonable to think that if a node is close enough to a gateway with a good link it is not necessary to always transmit data at maximum power and lowest data rate. "By shifting the data to a higher rate, the time on air is shortened opening up more potential space for other nodes to transmit." [37] The adaptive data rate is implemented with at least one receive time window on the node side which is used to synchronize. "A network can be deployed with a minimal amount of infrastructure, and as capacity is needed, more gateways can be added, shifting up the data rates, reducing the amount of overhearing to other gateways, and scaling the capacity." [37]

Device Classes

Not all the nodes end-devices have the same requirements as they vary with the application. LoRaWAN implements three different device classes for the particular application profiles where dissimilar network downlink communication latency and battery lifetime are desired.

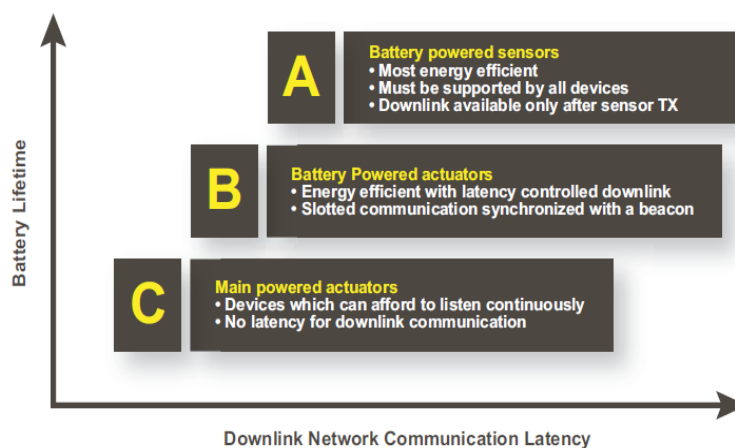


Figure 2.8: LoRaWAN device classes.[37]

Bi-directional end-devices (Class A): This type of nodes are the ones with the best battery lifetime. They allow bi-directional communications as each uplink transmission from the nodes is followed by two downlink receive time windows. Transmission moment is completely defined by the node needs, and after that it is the unique moment that the gateway has to transmit to the node. "Downlink communications from the server at any other time will have to wait until the next scheduled uplink."

Bi-directional end-devices with scheduled receive slots (Class B): "In addition to the Class A random receive windows, Class B devices open extra receive windows at scheduled times." This type of nodes have a shorter battery lifetime than Class A due to periodically having to 'wake up' to 'listen'

to the server. "In order for the end-device to open its receive window at the scheduled time, it receives a time-synchronized beacon from the gateway. This allows the server to know when the end-device is listening." [37]

Bi-directional end-devices with maximal receive slots (Class C): End-devices of Class C have almost continuously open receive windows, only closed when transmitting and therefore the worst battery lifetime compared with other classes.

Class A end-devices is what best fits the application of the present work, as it is intended to have the nodes uplinking every hour on demand, without the necessity of downlink communications most of the time.

Security

In order to bring security to communication "LoRaWAN utilizes two layers of security: one for the network and one for the application. The network security ensures authenticity of the node in the network while the application layer of security ensures the network operator does not have access to the end user's application data. AES encryption is used with the key exchange utilizing an IEEE EUI64 identifier."

LoRaWAN regional specifications

There are some variants on LoRaWAN specification for regional spectrum allocations and regulatory requirements, depending on the region. The LoRaWAN specification for Europe, United States, China, South Korea, Asia, and Australia are defined, but other regions are still being defined by the technical committee. As for South America, and Uruguay in particular, there is no a particular regional specification defined, but the US regional specifications may apply according to [38].

	EU	EU	US	CN	CN
Frequency band	433 MHz	863-870 MHz	902-928 MHz	470-510 MHz	779-787 MHz
Channels	16	16	64+8+8	96+48	16
Channel BW	125/250 kHz	125/250 kHz	125/500 kHz	125/250 kHz	125/250 kHz
Max. TX Power	+10dBm	+20dBm	+30dBm	+17dBm	+10Bm
Data Rate	250bps-11kbps	250bps-11kbps	980bps-21.9kbps	250bps-5.5kbps	250bps-11kbps
Max. payload	51-242	51-242	11-242	51-242	51-242

Table 2.4: LoRaWAN specifications depending on region.[39]

LoRaWAN for Europe

LoRaWAN defines sixteen channels, the first three channels correspond to 868.1, 868.3, and 868.5 MHz / DR0 to DR5 and must be implemented in every end-device. The maximum output power allowed by ETSI in Europe is +20 dBm, with the exception of the G3 band which allows +27 dBm. There are duty cycle restrictions under ETSI but no max transmission or channel dwell time limitations.

LoRaWAN for North America

”The ISM band for North America is from 902-928 MHz. LoRaWAN defines 64, 125 kHz uplink channels from 902.3 to 914.9 MHz in 200kHz increments. There are an additional eight 500 kHz uplink channels in 1.6 MHz increments from 903 MHz to 914.9 MHz. The eight downlink channels are 500 kHz wide starting from 923.3 MHz to 927.5 MHz. The maximum output power in North America 902-928 MHz band is +30 dBm but for most devices +20 dBm is sufficient. Under FCC there are no duty cycle limitations but there is a 400 ms maximum time per channel.”

Feature	LoRaWAN	Narrow-Band	LTE-Cat1 2016	LTE-CatM 2018	NB-LTE 2019
Modulation	SS Chirp	UNB/GFSK/BPSK	OFDMA	OFDMA	OFDMA
Rx BW	125/500 kHz	100 Hz	20 MHz	1.4-20 MHz	200 kHz
Data rate	290bps-50kbps	100bps	10Mbps	200kbps-1Mbps	20kbps
Max. msgs/day	Unlimited	140 msg/day	Unlimited	Unlimited	Unlimited
Max. output power	30dBm	20dBm	23-46dBm	23-30dBm	20Bm
Link budget	154 dBm	151 dBm	130 dBm	146 dBm	150 dBm
Battery lifetime (2000 mAh)	105 mths	90 mths		18 mths	
Power efficiency	Very high	Very high	Low	Medium	Med high
Interference immunity	Very high	Low	Medium	Medium	Low
Coexistence	Yes	No	Yes	Yes	No
Security	Yes	No	Yes	Yes	Yes
Mobility	Yes	Limited	Yes	Yes	Limited
Localization	Yes	No	No	No	No

Table 2.5: LPWAN protocols comparison.[37]

2.1.3.2 SX1276 Transceiver

The SX1276 transceiver is the integrated circuit used to implement the LoRa long range communication. It features a modem that provides ultra-long range spread spectrum communication, high interference immunity, and very low current consumption.

The long range capability is based on the combination of good sensitivity (-148 dBm) and +20 dBm transmission power. The SX1276 not only has got a LoRa modem but also FSK modem integrated in the same package. The modem type, user configurable LoRa parameters (as bandwidth, spreading factor, coding rate, etc.), and other parameters, are all configurable through internal registers.

”LoRa also provides significant advantages in both blocking and selectivity over conventional modulation techniques, solving the traditional design compromise between range, interference immunity and energy consumption.”[40].

Some of the SX1276 features are listed below [40]:

- LoRa Modem
- 168 dB maximum link budget
- +20 dBm - 100 mW constant RF output vs. V supply
- +14 dBm high efficiency PA

- Programmable bit rate up to 300 kbps
- High sensitivity: down to -148 dBm
- Excellent blocking immunity
- Low RX current of 9.9 mA, 200 nA register retention
- Fully integrated synthesizer with a resolution of 61 Hz
- FSK, GFSK, MSK, GMSK, LoRa and OOK modulation
- Built-in bit synchronizer for clock recovery
- Preamble detection
- 127 dB Dynamic Range RSSI
- Automatic RF Sense and CAD with ultra-fast AFC
- Packet engine up to 256 bytes with CRC
- Built-in temperature sensor and low battery indicator

For flexibility, the user can configure the spread spectrum modulation, bandwidth (BW), spreading factor (SF), and error correction rate (CR).

The SX1276 offers bandwidth options ranging from 7.8 kHz to 500 kHz with spreading factors ranging from 6 to 12, and covering all available frequency bands.

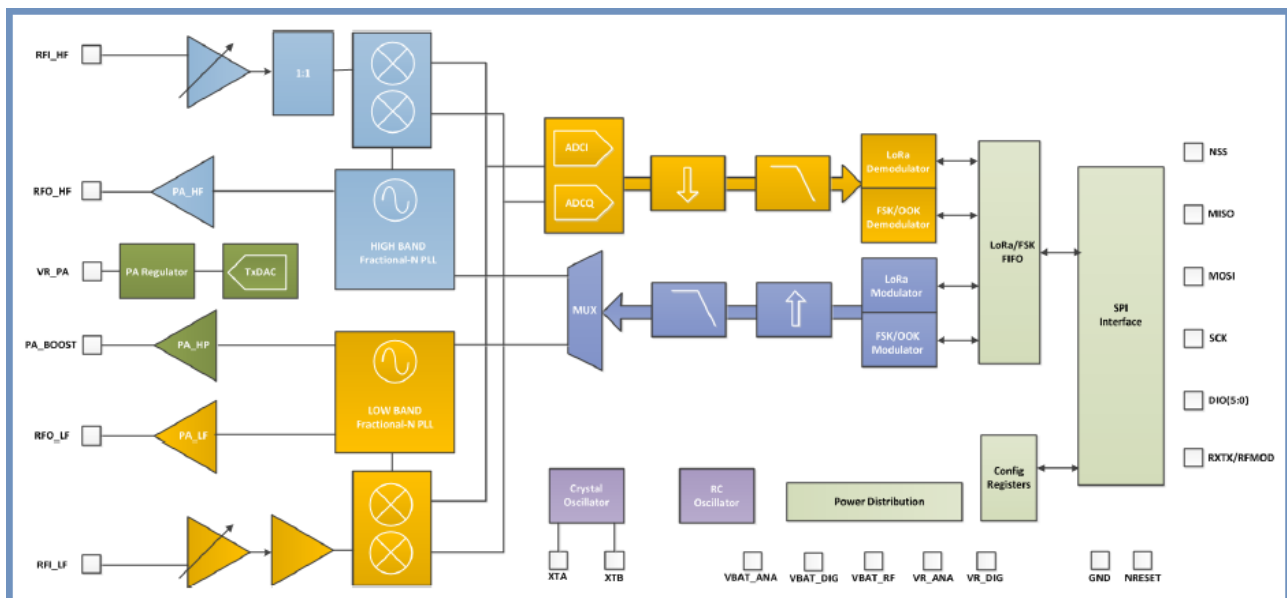


Figure 2.9: SX1276 simplified block diagram.[40]

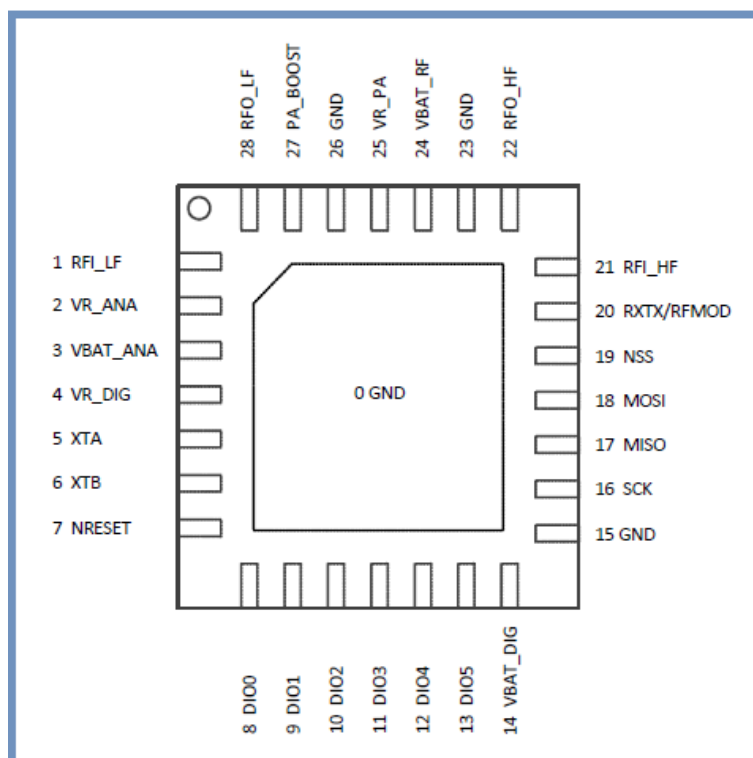


Figure 2.10: SX1276 pin diagram.[40]

Pin No.	Name	Type	Description
0	GND	-	Exposed ground pad
1	RFLF	I	RF input for bands 2 and 3
2	VR_ANA	-	Regulated supply voltage for analog circuitry
3	VBAT_ANA	-	Supply voltage for analog circuitry
4	VR_DIG	-	Regulated supply voltage for digital blocks
5	XTA	IO	XTAL connection or TCXO input
6	XTB	IO	XTAL connection
7	NRESET	IO	Reset trigger input
8	DIO0	IO	Digital IO, software configured
9	DIO1DCLK	IO	Digital IO, software configured
10	DIO2DATA	IO	Digital IO, software configured
11	DIO3	IO	Digital IO, software configured
12	DIO4	IO	Digital IO, software configured
13	DIO5	IO	Digital IO, software configured
14	VBAT_DIG	-	Supply voltage for digital blocks
15	GND	-	Ground
16	SCK	I	SPI Clock input
17	MISO	O	SPI Data output
18	MOSI	I	SPI Data input
19	NSS	I	SPI Chip select input
20	RXTXRF_MOD	O	RxTx switch control: high in Tx
21	RFLHF (GND)	I(-)	RF input for band 1 (Ground)
22	RFO_HF (GND)	O(-)	RF output for band 1 (Ground)
23	GND	-	Ground
24	VBAT_RF	-	Supply voltage for RF blocks
25	VR_PA	-	Regulated supply for the PA
26	GND	-	Ground
27	PA_BOOST	O	Optional high-power PA output, all frequency bands
28	RFO_LF	O	RF output for bands 2 and 3

Table 2.6: SX1276 pin functions description.

2.1.4 Microcontroller: MSP430

To configure, control and data processing, the MSP430FR5969 microcontroller from Texas Instruments is used. Among the vast universe of microcontrollers available at the market, the MSP430FR5969 was selected for its ultra low power characteristic due to its Ferroelectric memory (FRAM).

Ferroelectric Random Access Memory (FRAM) is an ultra-low power nonvolatile memory technology with write speeds similar to static RAM (SRAM), is very flexible, and can be used for program or data memory. It can be written to in a bit-wise fashion and with virtually unlimited write cycles.

The MSP430FR5969 microcontroller "combines embedded FRAM and an ultra-low-power system architecture, allowing to increase performance at lowered energy budgets." The FRAM technology not only offers the same advantages of SRAM (speed, flexibility, and endurance) but also the stability and reliability of flash at much lower power.

"The MSP430 ULP FRAM portfolio consists of a diverse set of devices featuring FRAM, the ULP 16-bit MSP430 CPU, and intelligent peripherals targeted for various applications. The ULP architecture showcases seven low-power modes, optimized to achieve extended battery life in energy-challenged applications." [41]

Some features of the MSP430FR5969 are listed below [41]:

- 16-Bit RISC Architecture up to 16 MHz Clock
- Wide Supply Voltage Range: 1.8 V to 3.6 V
- Optimized Ultra-Low-Power Modes
 - ◊ Active Mode: Approximately 100 μA MHz
 - ◊ Standby (LPM3 With VLO): 0.4 μA (Typical)
 - ◊ Real-Time Clock (LPM3.5): 0.25 μA (Typical)
 - ◊ Shutdown (LPM4.5): 0.02 μA (Typical)
- 64KB of Nonvolatile Memory (Ultra Low Power Ferroelectric RAM)
- 2KB of SRAM
- Unified Memory = Program + Data + Storage in one single space
- 10^{15} Write Cycle Endurance
- 32-Bit Hardware Multiplier (MPY)
- Real-Time Clock (RTC) With Calendar and Alarm Functions
- Edge-Selectable Wake From LPM on All Ports
- Programmable Pullup and Pulldown on All Ports
- SPI at Rates up to 10 Mbps
- Hardware UART and I2C Bootstrap Loader (BSL)
- Fixed-Frequency DCO With 10 Selectable Factory-Trimmed Frequencies

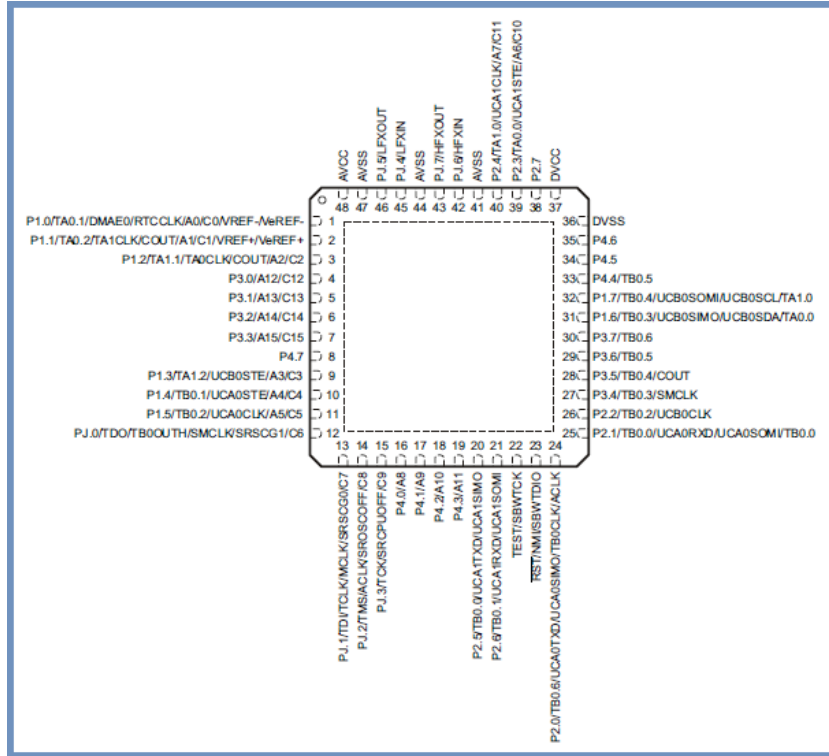


Figure 2.11: MSP430FR5969 RGZ package, pin diagram.[41]

2.1.4.1 Requirements

From the specifications defined at 1.3 and having the accelerometer and LoRa transceiver elected, it is known what kind of peripherals the microcontroller needs, and hence the microcontroller’s pins quantity and what functionality in each pin is used.

The functions needed by the microcontroller are:

- Communicate via SPI with the accelerometer to configure and get data from it.
- Communicate via SPI with the LoRa transceiver to configure and send data through it.
- Control signals for accelerometer and LoRa transceiver.
- Brown Out detector in case of supply voltage drop.
- Internal RTC if hour and date should be kept.
- Watch dog timer (WDT).
- Deep low power state.

Memory size needed could not be known at a start of the project as it depends on firmware stack, but at [42] a reference table could be observed as a reference start point (see Table 2.7):

The microcontroller programming is developed in C language over the **Code Composer Studio** IDE, which is an IDE provided by Texas Instruments and is based on Eclipse. Firmware architecture is explained in detail on section 2.2. As for the hardware programmer, the BSL 'Rocket' loader, explained later in Appendix E, is used.

Parameters	Minimum Settings	Recommended Settings
RAM	4 KB	8 KB
Flash	32 KB	64 KB
AES 128 bits	AES decryption in software	AES HW decryption block
Radio DIOs connected	DIO0, DIO1, DIO2	DIO0, DIO1, DIO2, DIO3
SPI (4 wires: SCK, MOSI, MISO, NSS)	mandatory	mandatory
RTC (32.768 kHz XTAL)	Recommended for accurate time keeping	Mandatory for low-power Class B implementation
IEEE 64-bit Extended Unique Identifier (EUI-64)	Programmed in ROM	Hardcoded in MCU

Table 2.7: MCU minimum requirements for LoRaWAN implementation.

2.1.5 Power Supply

This system is intended to have very low power consumption, and thus it is mandatory to be a battery-powered device, non rechargeable for the sake of robustness, and with a duration of a couple of months at least, but ideally years.

2.1.5.1 Power consumption and battery election

Theoretical current consumption estimation

Estimating consumption of the circuit in the first stage of the design is an important task to determine the power requirements of it. To make this estimation, analysis is divided in two: a worst case scene, which corresponds to the device in a wake up state and transmitting data via LoRa wireless communication (peak current), and a normal state where the system is almost all the time in a sleep state, with only the accelerometer running and sampling into its FIFO buffer. For both cases, current consumption could be estimated from datasheets:

- Accelerometer running at normal noise level: $1.8 \mu A$ [36].
- MSP430 running at 8 MHz: $1220 \mu A$ [41].
- MSP430 in LPM4 (Deep Low Power Mode): $0.5 \mu A$
- LoRa IC transmitting at maximum power: $120 mA$ [40].
- LoRa IC in sleep state: $0.2 \mu A$
- RF Switch current consumption: $9 \mu A$ [43].

Therefore, the worst case scene has a total current consumption of $121.231 mA$, while the normal scene could be estimated with a current consumption of $11.5 \mu A$. It is notorious with a naked eye that the used RF Switch is not a good election, as it represents the 78.3 % of the total current consumption of the normal state and must be replaced in future designs.

Battery

At a first stage, and due to the current consumption estimations, it was elected to use a standard 2032 coin cell from Maxell as battery power supply. These batteries are primary batteries with following specifications:

- Material: Manganese dioxide-Li/Organic Electrolyte.
- Nominal capacity: 220 mAh (typical).
- Nominal voltage: 3.0 V (mean voltage at a discharge current of 0.2 mA).
- Operating temperature range: -20°C to $+85^{\circ}\text{C}$.
- Dimensions: Diameter 20.0 mm, Height 3.2 mm.[44]

While not transmitting data, only acquiring acceleration data and processing it, the battery seemed to be appropriate for the application, but when data transmission occurred, it was observed that the microcontroller was reset.



Figure 2.12: Lithium coin cell battery of 3.0 V, 220 mAh.

After some investigation, it was noticed that it is a very common problem for new IoT sensors which need to transmit data periodically and battery powered. The reset problem is due to the high current peaks at the transmission moment, and the high series resistor of the battery (around $1k\Omega$), causing a power supply voltage drop below the minimum needed.

Many application notes treat this topic (as [45] and [46]) and all of them recommend a common technique to handle high peak currents which consists in using a capacitor to offload the power source. As it is clearly explained in [45] "during high current periods the capacitor will act as the primary power source, while during low current periods the battery will be the primary power source and recharge the capacitor". Therefore, the size of the capacitor will depend on the battery's internal resistance and the load profile. Once this information is available, it is quite simple to dimension a suitable capacitor.[45]

Capacitor sizing [45]

To facilitate the sizing of the capacitor, a simplification is made: During the high current states the battery voltage is fixed at V_{min} . This will cause an error on the safe side, meaning that the battery will deliver slightly more energy than calculated.

To calculate the capacitance, the focus is made on the high load states (processing and Tx). The formula is given as [46]:

$$C = \frac{\Delta Q}{V_{max} - V_{min}} \quad (2.1)$$

where

$$\Delta Q = Q_{dis} - \frac{V_{min}}{R_i} t_{tot} \quad (2.2)$$

Q_{dis} is the total energy consumed during the high load states and for this calculation it is represented as $Q_{dis} = \Sigma I_n * t_n$. The peak current is not taken into account for the previous representation, instead it is the total energy consumed during the high load states. V_{min} is chosen by design to match the circuit's lowest operating voltage. R_i is the maximum internal resistance the circuit should be able to manage. V_{max} is the voltage over the capacitor at the very start of the discharge pulse at the battery's end of life, and must initially be estimated. Further down V_{max} can be refined. In this case the following values were chosen:

- $V_{max} = 2.6V$
- $V_{min} = 2.0V$
- $R_i = 1k\Omega$

The resulting calculation is as follows:

$$C = \frac{1.18mA * 11.3ms + 89.4mA * 9.55ms - \frac{2.0V}{1k\Omega} * 11.3ms + 9.55ms}{2.6V - 2.0V} = 1.37mF \quad (2.3)$$

which is a very high value for this application and will led in elevated costs and in parasitic current consumption equal or higher than the rest of the device itself.

To correct the problem, a new battery was chosen with enough peak current performance, low series resistance, and a moderate cost adequate for this product. The new battery selected, part number CR024032 from MinMax (China), has the following characteristics and is shown at Figure 2.13:

- Material: Manganese dioxide-Li/Organic Electrolyte.
- Nominal capacity: 400 mAh (typical).
- Nominal voltage: 3.0 V (mean voltage at a discharge current of 1.0 mA).
- Operating temperature range: -20°C to +60°C.
- Max. pulse current: 150 mA (obtained at 1.8 V when pulse for 15 sec. 50% discharge depth.)
- Max. continuous discharge current: 80 mA.
- Dimensions: Length 39.0 mm, Width 30.0 mm, Height 2.3 mm.[47]



Figure 2.13: Lithium battery of 3.0 V, 400 mAh.

2.1.5.2 Power supply

For simplicity reasons, and because all integrated circuits used in the design tolerate the same supply voltage (between 1.8 V and 3.3 V), there is no need to use a voltage regulator. Therefore, the power supply is limited to the battery and a few capacitors to increase stability and to supply peak currents in transmission states.

Although it is not implemented in this work, a DC-DC step down converter for low power applications could be used to improve battery life. Power is reduced when reducing supply voltage to 1.8 V or 2.0 V (all components used work with these levels). To do so, the TPS62740 DC-DC step down converter [48] from Texas Instruments could be used. Among its characteristics are:

- Input voltage range V_{in} from 2.2 V to 5.5 V.
- Typ. 360 nA quiescent current.
- Up to 90% efficiency at $10\mu A$ output current.
- Up to 300 mA current output.
- Up to 2 MHz switching frequency.
- 16 Selectable output voltages in 100 mV steps between 1.8 V to 3.3 V.

2.1.6 Antenna

Two different PCB designs were made: one with a chip antenna and other with a helical antenna, in order to compare performances and reach the best antenna type for this application. Both antennas are small in order to fit in the collar case and for practical reasons, it is not convenient to have an external antenna on the cow's neck. However it is expected to have a bit worse results than with external antennas due to their sizes.

Figure 2.14 shows both antennas and Table 2.8 compares them.

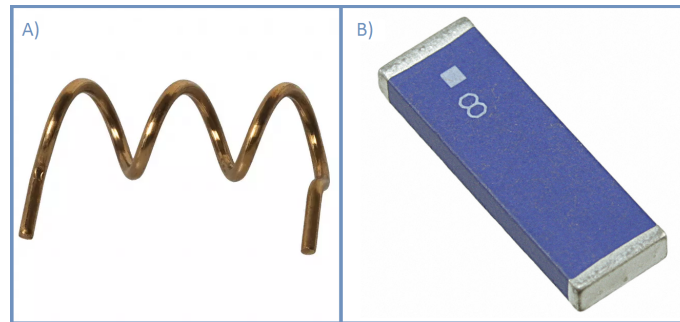


Figure 2.14: Both antennas used. A) Helical antenna. B) Chip antenna.

Parameters	Chip Antenna	Helical Antenna
Part number	ANT1204LL05R0915A	ANT-916-HETH
Frequency (CenterBand)	915 MHz	916 MHz
Frequency Range	905 MHz - 925 MHz	865 MHz - 965 MHz
Gain	3.32 dBi	2.4 dBi
Mounting Type	Surface Mount	Through Hole

Table 2.8: Comparison of the principal features of the antennas.

2.1.7 Layout design and PCB

Figure 2.18 shows the final result on PCB design. It is a 74.0 mm x 34.0 mm x 1.6 mm, 4 layer board. Dimensions were established based on a plastic case from *Hammond Manufacturing* (Part Number 1551K) already available at BQN.

Special care was taken on the wireless communication front-end. The design of the RF section of the circuit, was based on the guidelines in [49], that explains design criteria for the IC XE / SX1200, which has a similar antenna front-end to SX1276, so the same criteria applies (see Figure 2.15).

A 4-layer design was chosen, since according to the document, offers several advantages over a 2 layers design:

- Placing a distributed power plane between 2 ground plane layers enables an evenly distributed RF decoupling capacitance between the supply and ground. In addition, the power plane provides a very low impedance trace at radio frequencies.
- For an overall PCB thickness of 1.6 mm, the gap between the PCB component and routing layer and the first ground plane layer allows for distributed Microstrip traces to be employed. Similarly for RF routing on the layer between the ground planes or well-decoupled power planes, stripline techniques can be employed to ensure that traces have the required characteristic impedance (typically 50 Ohm).

The power plane is surrounded by a ground trace or vias that connect the two ground traces together, thus preventing any radiated emissions at the board edge. The power plane is suppressed at the final stage of the TX matching network to prevent any parasitic coupling caused by radiated and reflected energy at this stage. Each of the 4 layers design could be observed at Figure 2.16.

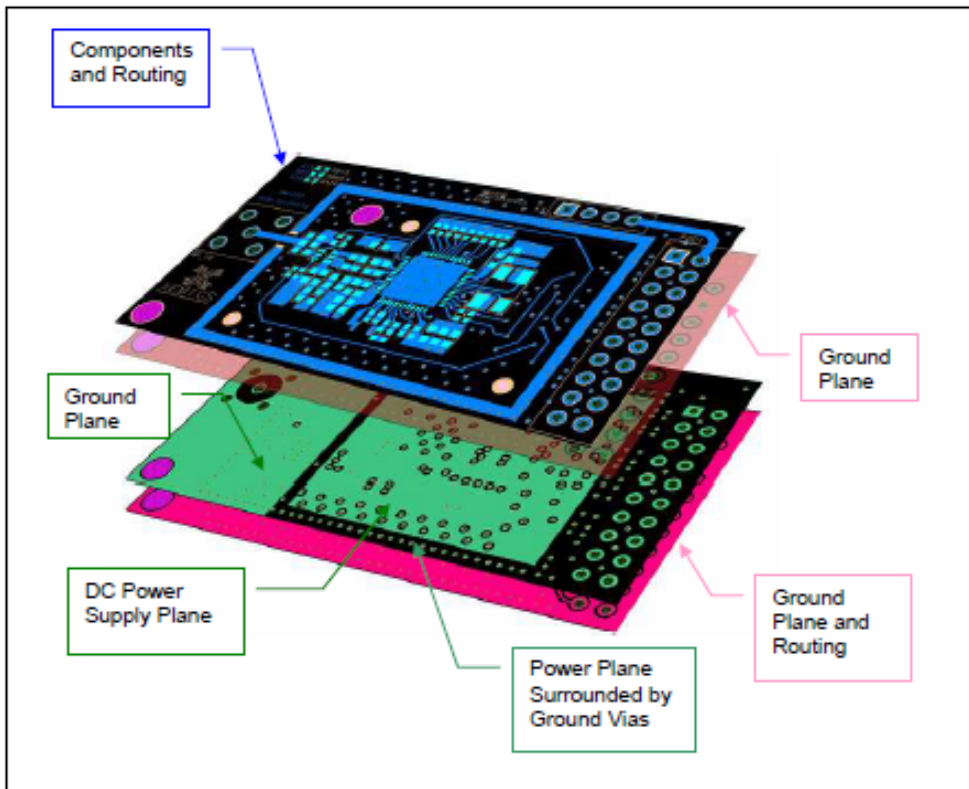


Figure 2.15: PCB design recommendations by Semtech.[49]

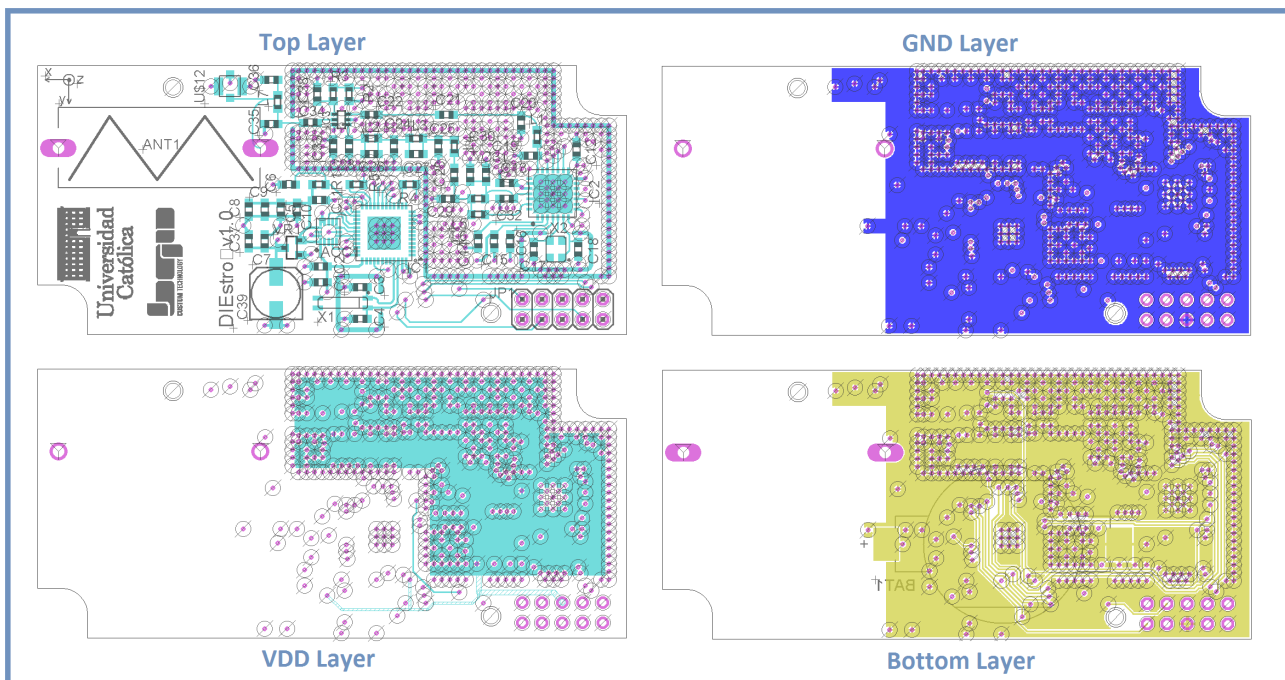


Figure 2.16: Four designed layers view (helical antenna PCB type).

2.1.7.1 PCB transmission lines

The following guidelines were used for antenna matching circuitry:

- Shorten tracks as short as possible.
- Decoupling capacitors as close as possible to the pins of the IC.
- Controlled impedance on tracks.

The model in Figure 2.17 was utilized for the calculation of the controlled impedance transmission lines.

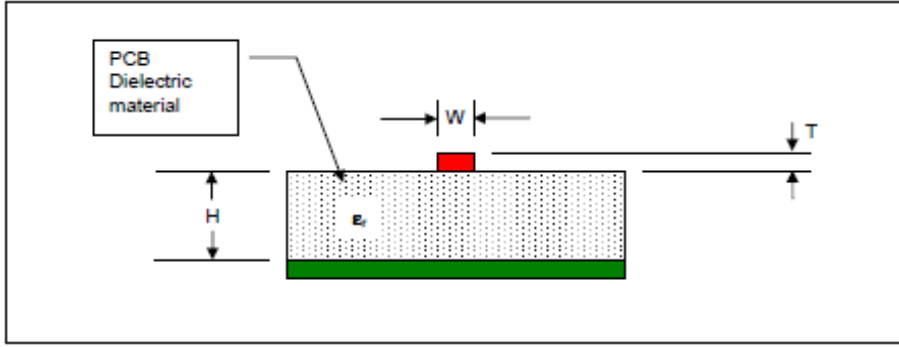


Figure 2.17: Matched impedance calculation model.[49]

The required width of the PCB trace, W , it is first necessary to calculate the effective dielectric constant, ϵ_{eff}^2 . The effective dielectric constant is required because part of the field generated by the conductor will exist in air ($\epsilon = 1$) and part in the dielectric material. Assuming that the thickness of the trace, T , is small compared to the height of the dielectric ($T/H < 0.005$), then ϵ_{eff} can be calculated using the following equations:

$$\left(\frac{W}{H}\right) < 1 \Rightarrow \epsilon_{eff} = \frac{\epsilon_r + 1}{2} + \frac{\epsilon_r - 1}{2} \left[\left(1 + 12\left(\frac{H}{W}\right)\right)^2 + 0.04\left(1 - \left(\frac{W}{H}\right)\right)^2 \right] \quad (2.4)$$

$$\left(\frac{W}{H}\right) > 1 \Rightarrow \epsilon_{eff} = \frac{\epsilon_r + 1}{2} + \frac{\epsilon_r - 1}{2} \left(1 + 12\left(\frac{H}{W}\right)\right)^2 \quad (2.5)$$

$$\left(\frac{W}{H}\right) < 1 \Rightarrow Z_0 = \frac{60}{\sqrt{\epsilon_{eff}}} \ln\left(8\frac{H}{W} + 0.25\frac{W}{H}\right) \quad (2.6)$$

$$\left(\frac{W}{H}\right) > 1 \Rightarrow Z_0 = \frac{\frac{120\pi}{\sqrt{\epsilon_{eff}}}}{\frac{W}{H} + 1.393 + 0.667\ln\left(\frac{W}{H} + 1.444\right)} \quad (2.7)$$

A controlled impedance of 50 Ohm is desired, $W > H$ is assumed, and H and ϵ_r are fixed defined by the technology of PCB manufacturer:

- $H = 0.2mm$
- $\epsilon_r = 4.29$

Therefore, from equations 2.5 and 2.7, W should be **0.2 mm** approx.

Impedance matching efforts were made during PCB design, but no measurements were made after the components were soldered. Thus it is not possible to affirm that the antenna is matched, and therefore a worse performance may result when trying to transmit data (shorter distances).

The conventional approach would be to measure the unknown impedance using a vector network analyzer (VNA) or other impedance measuring device. Then using analytic techniques (Smith Chart or computer simulation), develop the network that provides the required matching function. For the case of both LNA and Power Amplifier impedance matching however, simply measuring the device impedance and matching that impedance to the desired 50 Ohm load will not yield the best performance. In order to achieve the optimum source impedance for the LNA and load impedance for the PA, a technique referred to as "load pull" is generally used. This involves using an adjustable tuner which can provide a continuously variable impedance match from a 50 Ohm port to the LNA or PA port allowing independent adjustment of both the resistive and reactive components. The tuner is adjusted while monitoring critical performance parameters (receiver sensitivity, power output, current drain, harmonic content etc) until an optimum level of performance is achieved. Then the impedance of this tuner input is measured and that becomes the optimum LNA source or PA load impedance. A network is then developed that transforms 50 Ohms to this value [50].

Figure 2.18 shows the final PCB manufactured by PCBWay in China.

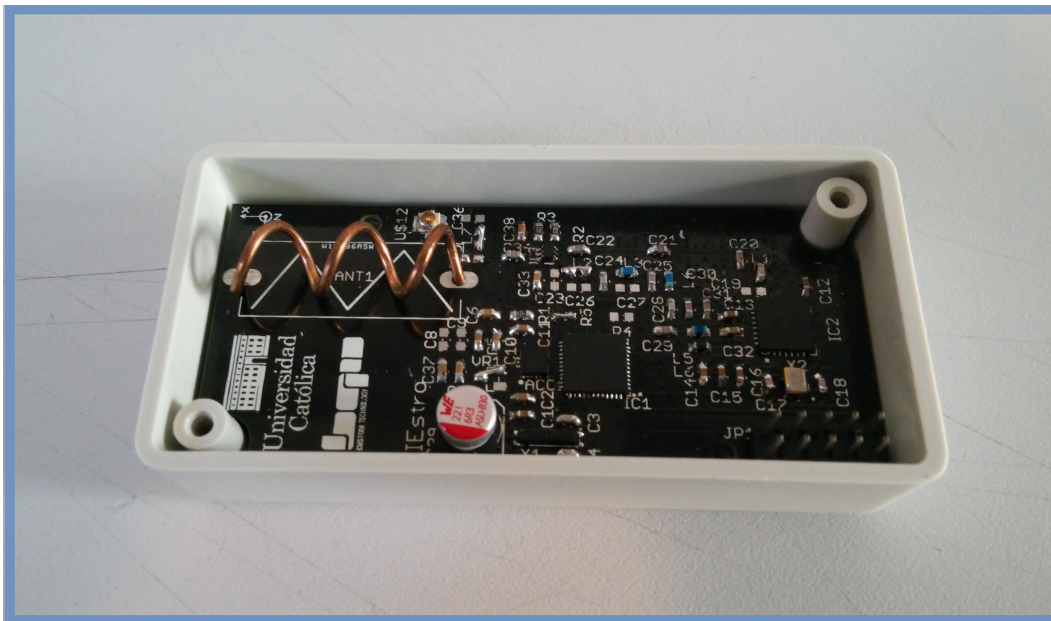


Figure 2.18: Final PCB in its case with all components mounted.

2.2 Firmware

In this section, the firmware of the MSP430FR5969 microcontroller is presented, from programming language to code architecture and data processing elections.

2.2.1 Code structure

The entire code allocated in MSP430FR5969 microcontroller FRAM memory is programmed in C language and developed with the Code Composer Studio IDE (based in Eclipse) provided by Texas Instruments (TI). Additionally to the IDE, compilers for MSP430 are provided by TI. Code Composer Studio v6.1.1 and TI v4.4.5 compiler were used.

C programming language is appropriate for the application complexity, it is not so low-level language as Assembly but with a good control of peripherals, time, size and speed.

In addition to the basic developers features of the IDE (compile, debug, etc.), **Code Composer Studio** together with the **Launchpad** development boards, provide a powerful tool called *EnergyTrace* technology with which energy and current consumption of the circuit can be monitored without the need of any additional tool.

All the program - accelerator drivers, LoRa drivers, data processing logic, etc. - is allocated in one Code Composer's project, called *DIEstro*, and program code was subdivided into 3 folders: app, cpu, and platform. The intention is to separate modules for specifically hardware control (platform) from the application modules (app) and the modules depending on the CPU used (cpu).

On Figure 2.19 the code tree structure can be observed. Detailed explanation on each module is at Appendix B.

2.2.1.1 Main file - Application

For the main application, a round-robing with interrupts architecture was chosen, where at start, all the hardware components are initiated and configured and then, a *while(1)* loop keeps all the rest of the program. Inside this loop, most of the time, the MCU and LoRa transceiver are in sleep mode, while the accelerator gets information and stores it at its FIFO buffer. Once the FIFO is full (each 6 secs), the MCU wakes up, clears the FIFO and process the data. When enough data is collected (each hour) data is processed and transmitted via LoRa wireless protocol. Figure 2.20 shows the flowchart of the program.

As it was said above, firstly, all the microcontroller peripherals specially dedicated to control and interact with the rest of the hardware are initiated and all the free pins are set as outputs at low digital level to save power. After that, SPI lines which communicate with the accelerometer are configured at 8 MHz, and many characteristics of the accelerometer are configured: acceleration range at 4 g, output data rate (ODR) at 25 Hz, antialiasing low-pass filter bandwidth at half of ODR (12.5 Hz), FIFO's maximum samples at 150 samples of each axis, each one of 2 bytes length (12 bits used), FIFO's interrupt on INT1 pin, and noise level at normal mode. Immediately after, all the callback functions associated with the SX1276 transceiver are assigned and configurable communications parameters are set: RF Frequency, Tx output power, bandwidth, spreading factor, coding rate, preamble length and payload length (all configured with SPI at 8 MHz). Once both ICs, accelerometer and LoRa transceiver, are configured, LoRa transceiver and the microcontroller are put in sleep and deep sleep mode, while the accelerometer is still running, sampling frequencies at 25 Hz and storing them into its FIFO buffer. When the FIFO reaches its watermark (150 samples), every 6 secs (150 samples/25 Hz), an interrupt is generated which wakes up the microcontroller. The microcontroller gets all the FIFO content via SPI, processes the data, decides if it has to send data, and comes back to the deep sleep mode, waiting for a new interrupt. Each hour data stored is processed and sent through LoRa wireless communication.

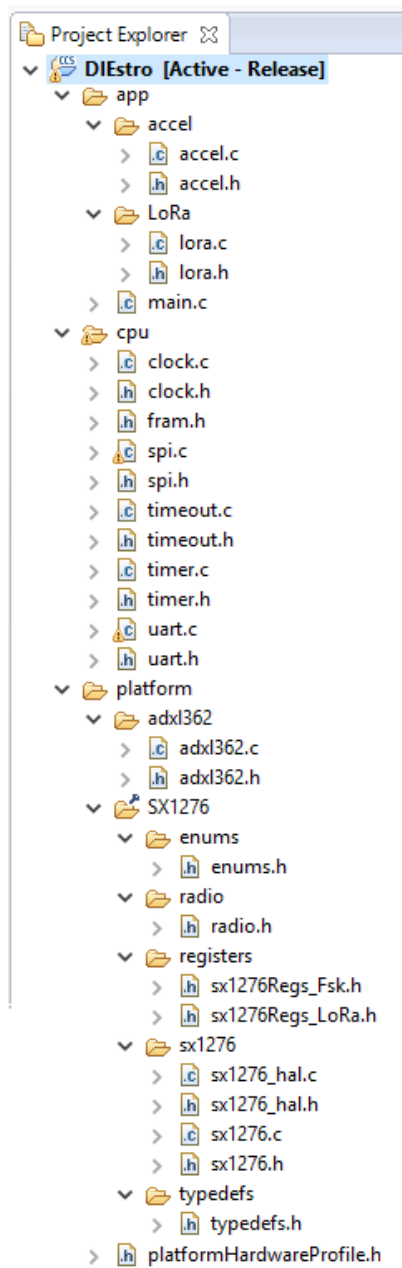


Figure 2.19: Firmware tree structure with all the modules implemented.

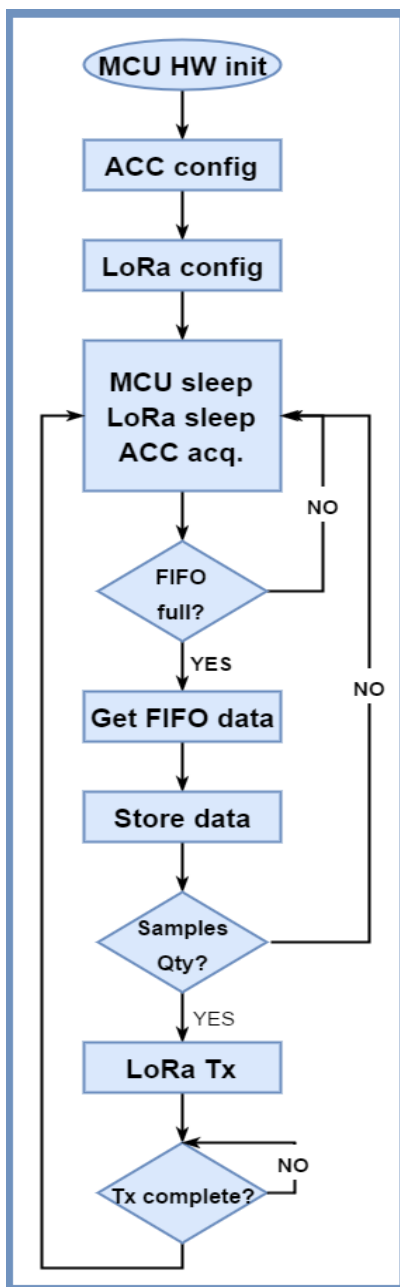


Figure 2.20: Basic flowchart of application program.

2.2.1.2 Data processing

As it was explained before in section 2.1.1, cow's activity was estimated of movements from 0.5 Hz to 7 Hz, therefore the acceleration samples are low-pass filtered by the accelerometer itself and high-pass filtered by software. Every acceleration sample for each axis is low-pass filtered by the accelerometer itself at half the sample rate, 12.5 Hz, for anti-aliasing. Then they are stored at the FIFO buffer (each acceleration data is represented in 12 bits (2 bytes) and every FIFO sample has information of the 3 axis, making a total of 6 bytes per sample). When FIFO is full (900 bytes corresponding to 150 samples), the MCU gets all the FIFO content, leaving the buffer free for a new period of data collection, calculates a mean value for each axis, and subtract its mean to each value (high-pass filtering) to avoid offset values due to gravity. After that, the square modulus of acceleration vector is calculated and stored in FRAM. Once per hour, all stored samples are averaged giving a mean value of square module accelerations from previous hour, and it is taken as an activity numeric representation. Figure 2.21 shows data processing block diagram representation.

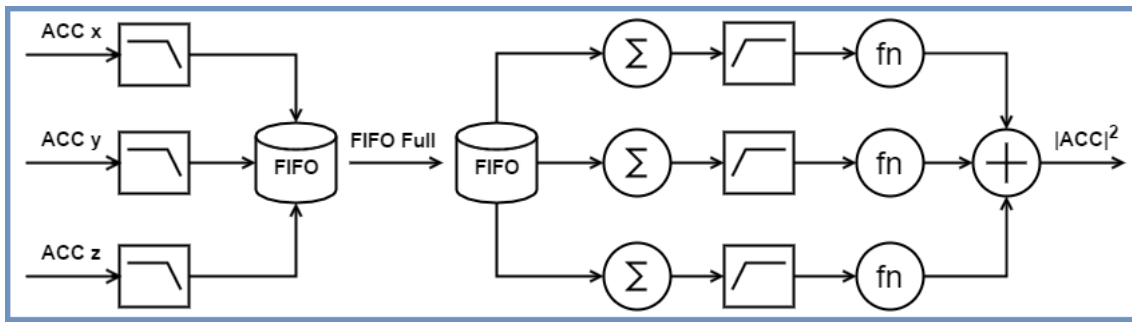


Figure 2.21: Data processing block diagram representation. fn represents the power or 2 operation.

2.2.2 Microcontroller Memory Layout

In section 2.1.4, a brief description of the FRAM present in the microcontroller was presented. As it was said in the previous section, all data collected and processed is stored in a FRAM buffer. In order to achieve this functional application, a customization of the FRAM space was made.

By default the 64 KB of FRAM in the microcontroller are distributed as shown on left side of Figure 2.22

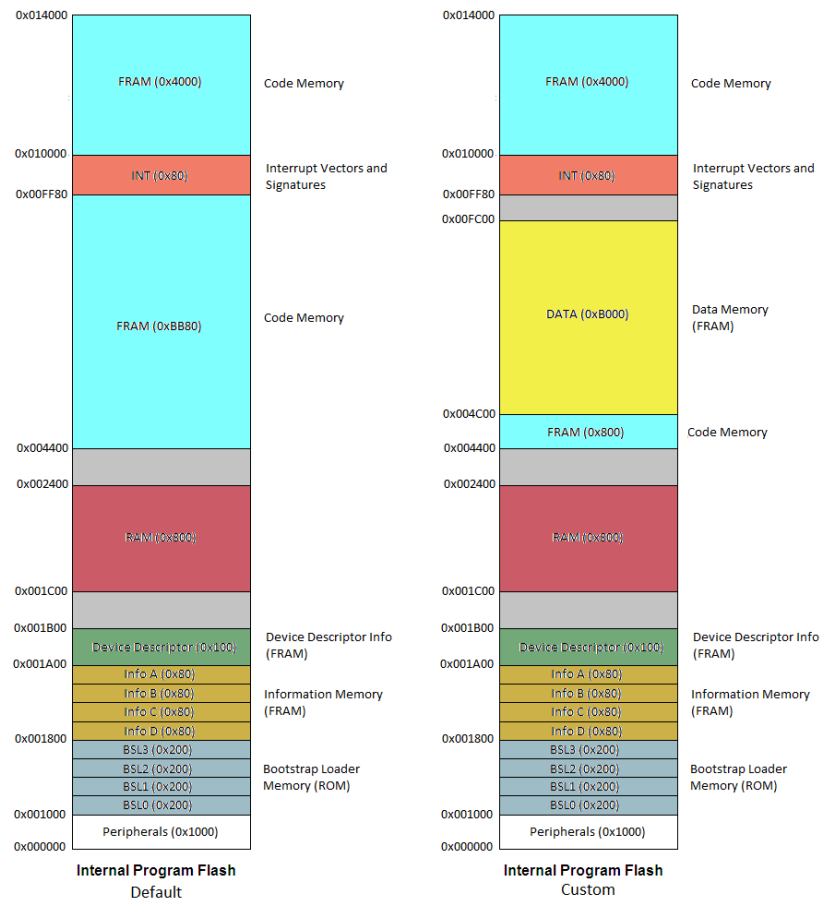


Figure 2.22: Left: Default memory layout. Right: Custom memory layout.

The customization consists of defining an area of 44 KB for data storage, where the acceleration values for the 3 axis and other important data (as the device serial number) is located. To make this change, the linker file and the MPU (Memory Protection Unit) boundaries of the microcontroller were modified. Detailed procedure for the changes is explained and a brief description of the FRAM present in the microcontroller is presented at Appendix D.

Chapter 3

Tests and results

This chapter lists and discusses what tests, to check the correct operation of the device, were implemented and what were the results of them.

The first test that was made was to check that the platform was working as expected: collecting acceleration samples, processing them, and transmitting the calculated acceleration values after a configurable period. Data was transmitted to another node configured as receiver and connected to a PC through a COM port, and the received values were graphed in real time through a custom software developed with Python programming language.

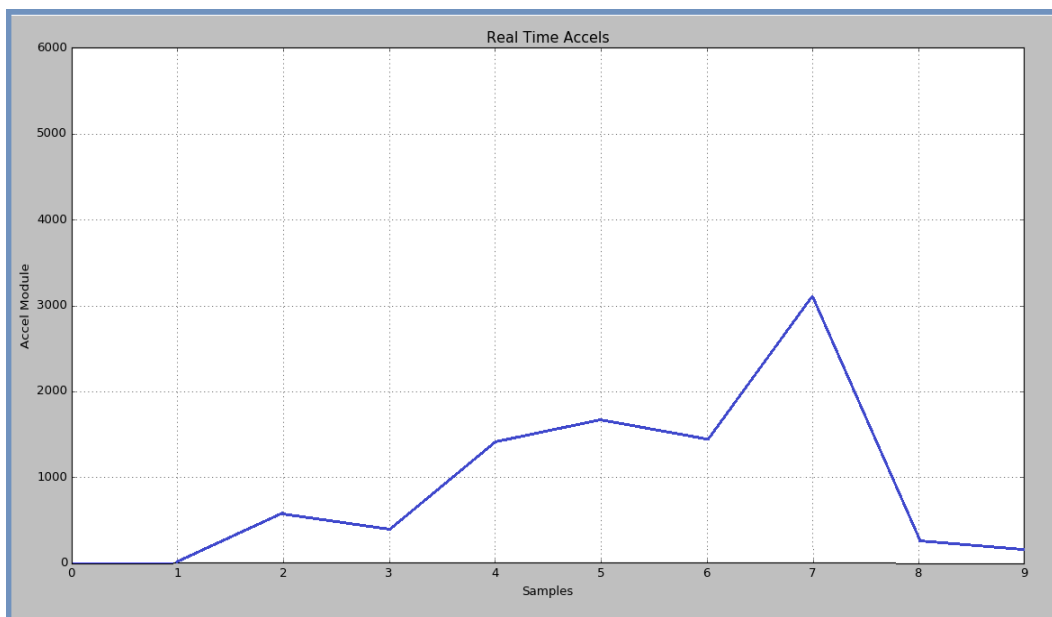


Figure 3.1: Simulated gateway received acceleration values. Software was developed with Python.

After the basic functionality was verified, the following tests were performed:

3.1 Power consumption

3.1.1 Practical measurement

In order to measure the power consumption, and due to the low currents present in the device, an external circuit was developed. This circuit was implemented with the *Electronics Explorer* board from Digilent [51] which has, among other things, configurable power supplies and four oscilloscope channels. Data extraction was made with the software associated to the test board, called *WaveForms* [52].

Figure 3.2 shows the circuit implemented while Table 3.1 lists the components values used.

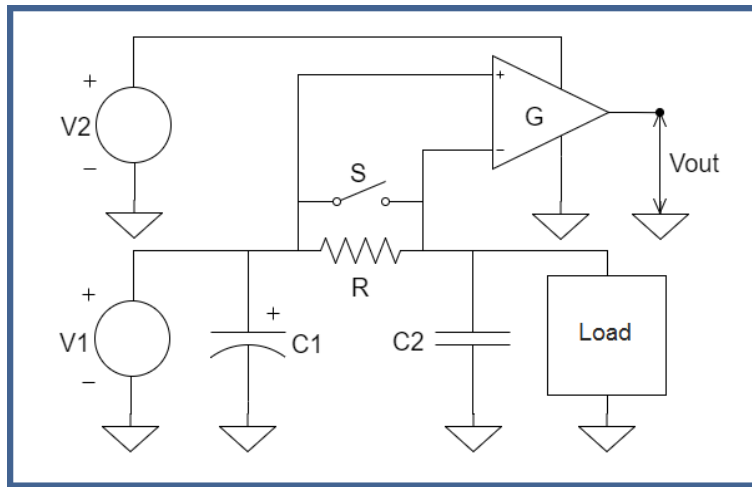


Figure 3.2: Power measurement circuit implemented. An instrumentation amplifier is used to measure differential voltage at resistor terminals.

Parameter	Value
V1	3.3 V
V2	5.0 V
C1	220 μF
C2	2.2 μF
R (Sleep)	1.5 k Ω
R (Processing)	7.5 Ω
R (Transmitting)	0.205 Ω
G	76

Table 3.1: Component values.

Switch S is used to allow the circuit to initialize and reach the desired state when closed, after that, the switch is opened and the current flowing through the resistor R could be measured as a voltage drop. With this test, not only the current could be measured, but also different important times, as the time the microcontroller is processing data from accelerometer, and the time data is being transmitted with LoRa wireless technology.

Different resistors value are used, each one for each different state, in order to have an amplified voltage drop of about 1.5 V.

An instrumentation amplifier implemented with three low offset OpAmps ($V_{offset} \approx 5\mu V$), with gain equal to 76, was used in order to measure differential voltage directly on terminals of the resistor.

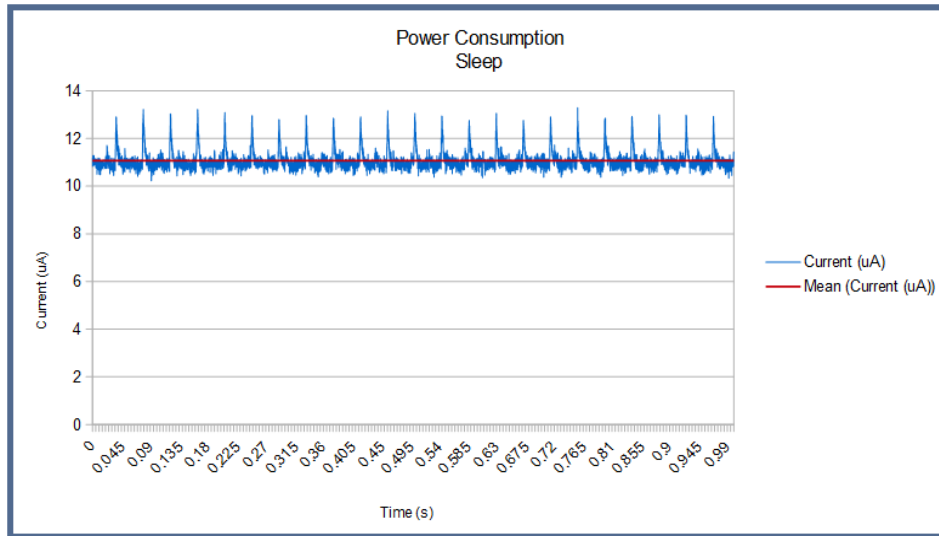


Figure 3.3: Current consumption during accelerations acquisition and microcontroller and LoRa in sleep states.

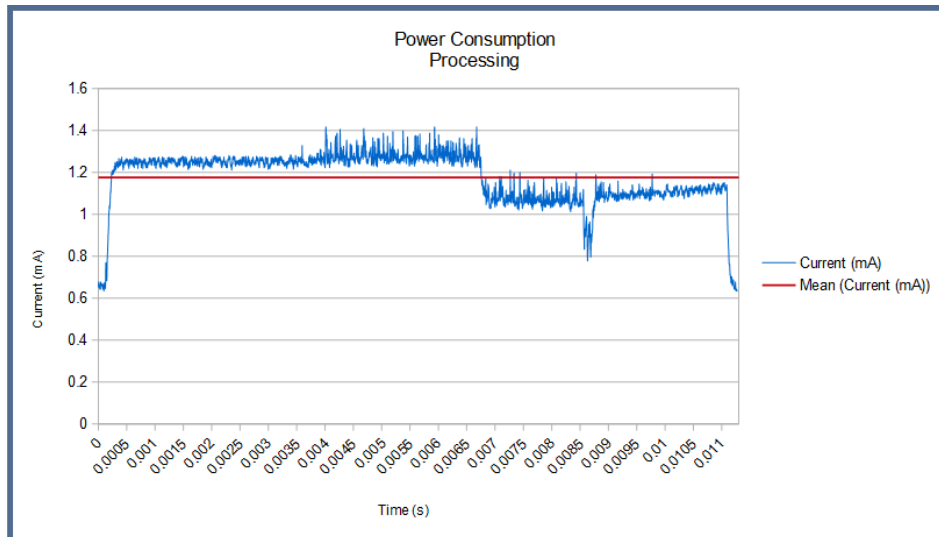


Figure 3.4: Current consumption during accelerations data processing.

From data extracted, mean current values and periodic time values were calculated and are listed in Table 3.2

Also there was used an amperimeter to contrast measures. Figure 3.6 shows the test board and amperimeter measure for sleep state.

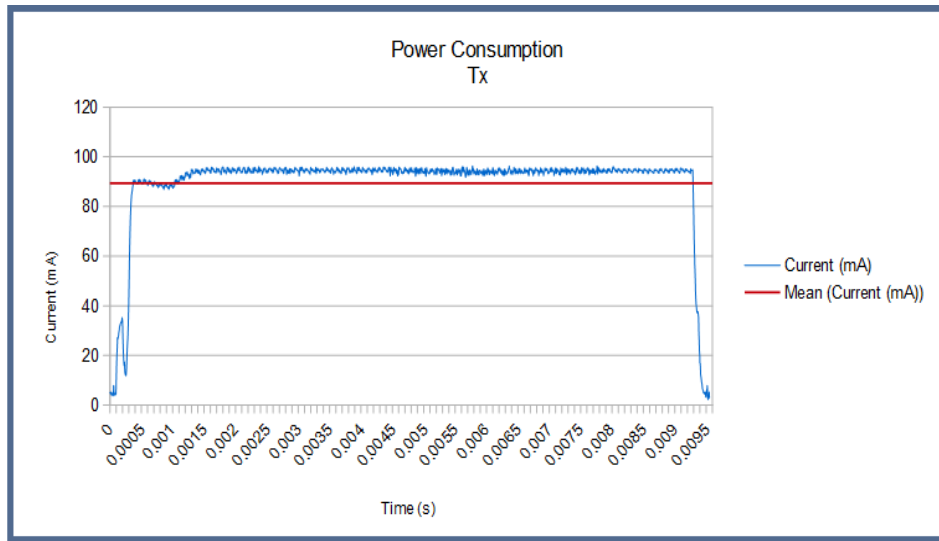


Figure 3.5: Current consumption during LoRa data transmission.

State	Current	Time
Sleep	11.07 μA	6 s
Processing	1.18 mA	11.27 ms
Transmitting	89.41 mA	9.55 ms

Table 3.2: Current and time measurements for the 3 different states. All the measures include 9 μA from the RF switch which will be lowered in future designs.

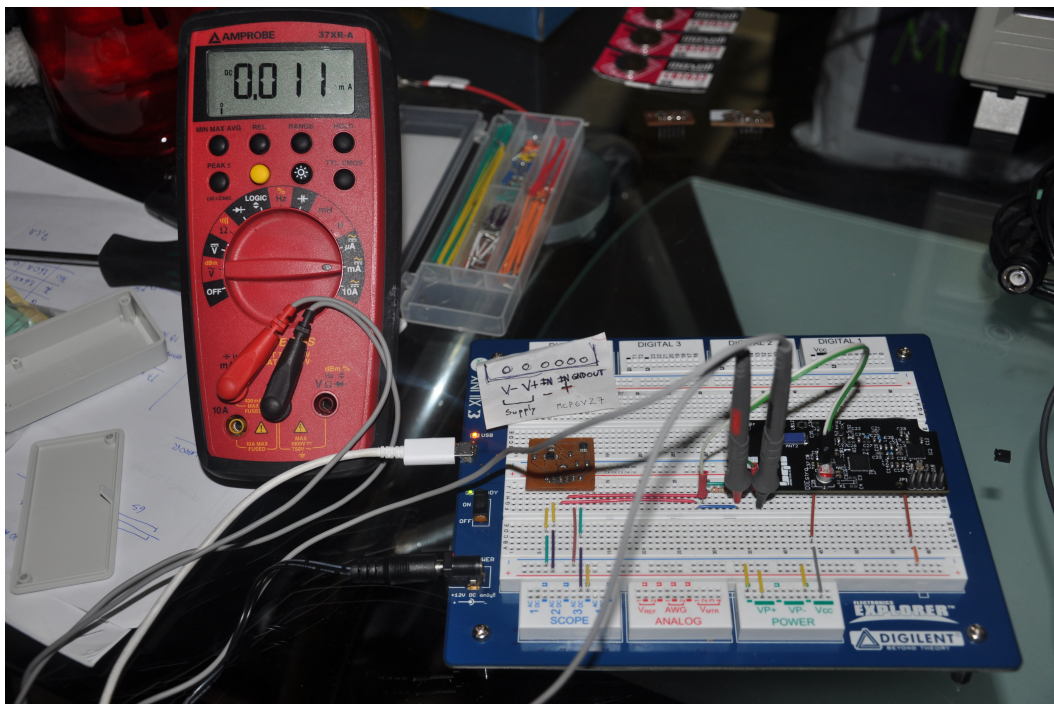


Figure 3.6: Current consumption measurement platform using an Electronics Explorer from Digilent where the circuit with the instrumentation amplifier was implemented.

3.1.2 Battery lifetime

From the previous measurements, a battery lifetime analysis could be performed. Since every 6 seconds the FIFO buffer of the accelerometer must be read and cleared, the sleep-processing period is always present, and therefore what has the highest impact in battery lifetime, due to its current consumption, is how often data is transmitted to the gateway. Different transmission periods were proposed to compare battery lifetime variation, shown on Table 3.3 and Figure 3.8, where it could be concluded that a very good solution is to transmit data every each hour, having a good relation between data acquisition and battery life duration. However, if necessary, transmissions every 10 minutes could be done without considerably affect battery lifetime and having more precise information from the server side.

Further analysis of battery lifetime can be found in chapter 4.

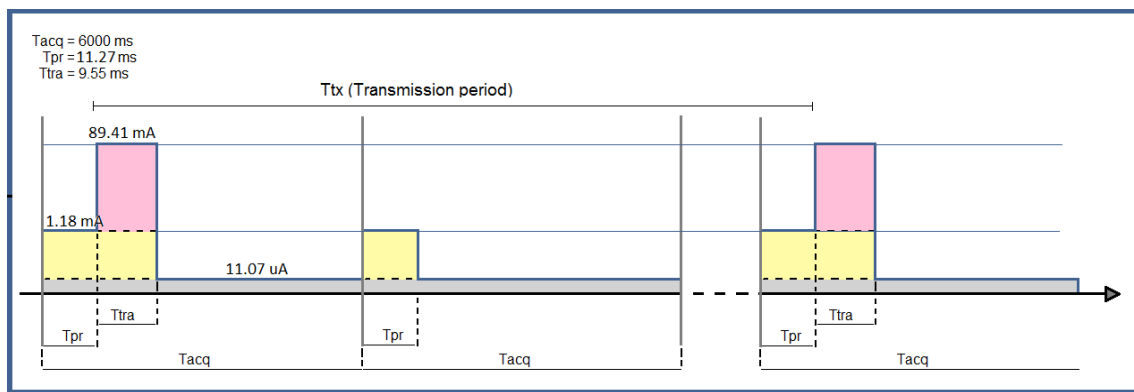


Figure 3.7: Average currents and times for each state.

Bat: 400 mAh			
Ttx (s)	I _{mean} (A)	Bat. (hs)	Bat. (days)
6 seg	1.475106E-04	2169.3	90
18 seg	5.272E-05	6070.1	252.9
30 seg	3.374E-05	9483.5	395.1
1 min	1.951E-05	16400.4	683.3
3 min	1.002E-05	31922.3	1330.1
10 min	6.704E-06	47734.4	1988.9
30 min	5.755E-06	55603.6	2316.8
1 hr	5.518E-06	57993.7	2416.4
1.6 hr	5.423E-06	59008.3	2458.7
2 hr	5.399E-06	59267.6	2469.5
3.3 hr	5.352E-06	59792.9	2491.4

Table 3.3: Battery lifetime depending on transmissions period (Ttx) and battery capacity. SF=7, BW=500 kHz, CR=1, Payload = 32 bytes.

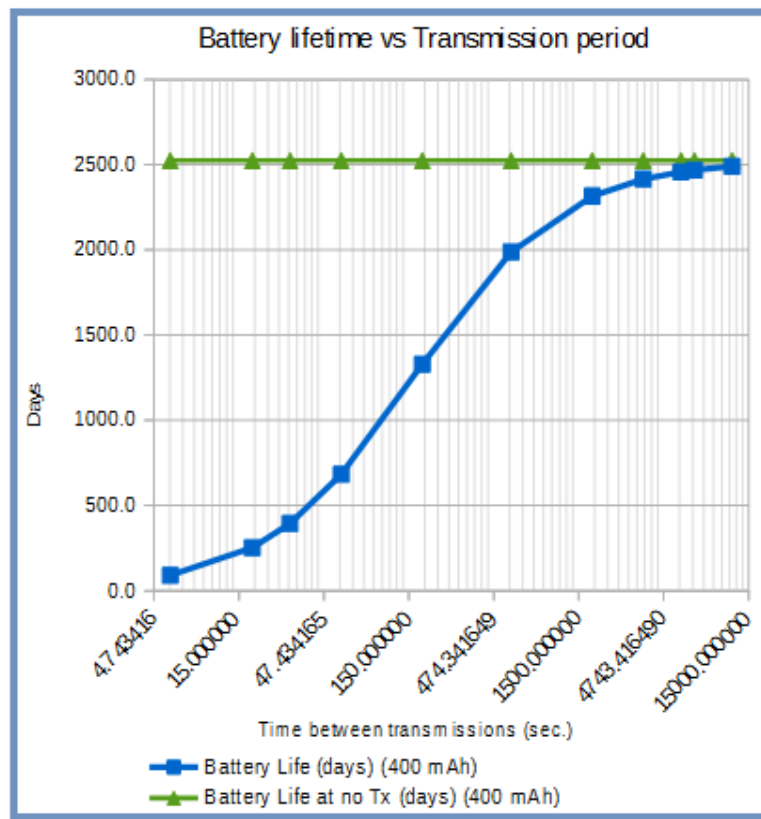


Figure 3.8: Battery lifetime vs Transmission periods.

3.2 LoRa communication

3.2.1 Data transmission time

The total time that the SX1276 LoRa transceiver is transmitting data depends on multiple factors, as spreading factor, coding rate, payload length, among others. Theoretical values were obtained from the *LoRa Calculator* software, which allows the user to vary different parameters and observe how they influence different aspects of the communication as total time transmitting, current consumption and estimated battery life.

Different scenarios were raised and theoretical results were compared with practical measures. To perform the measures an unused pin in the microcontroller was used as test pin. It was configured as digital output and its behaviour was the following: goes HIGH when starting to transmit data and goes LOW when data transmission finishes. Time intervals were measured with an oscilloscope and comparison between theoretical values and practical measures can be observed at table 3.4.

From Table 3.4 could be observed that spreading factor has an important impact on transmission time as moving from a SF of 7 to a SF of 12 transmission time increases more than 25 times. Coding rate has a small impact on transmission time compared to spreading factor. All the previous measures were done with a constant bandwidth of 500 kHz, in order to improve communication distance, bandwidth could be lowered while keeping SF at maximum and coding rate too. Appendix C shows how spreading factor and bandwidth affect transmission time.

From 3.4, could be concluded that LoRa Calculator tool accurately estimated transmission times based on different parameters and is a good reference starting point.

Parameters (s)	LoRa Calculator	Measured
SF=7, CR=1, PYLD=32	17.98 ms	19.0 ms
SF=7, CR=1, PYLD=8	9.02 ms	9.6 ms
SF=12, CR=1, PYLD=8	247.81 ms	258.7 ms
SF=12, CR=4, PYLD=8	296.96 ms	296.7 ms

Table 3.4: Data transmission times comparison between LoRa calculator simulation and practical measures. For all the measures the following parameters were constant: Explicit header mode, Tx Output Power (+20 dBm), Bandwidth (500 kHz), Preamble length (8 bytes).

3.2.2 Communication distance measurements

Several assays were made to determine LoRa communication maximum distance and compare the results with the distances promised by Semtech (2 km in a dense urban environment and 16 km in the countryside). As for this work there was not a LoRa gateway available, tests were developed establishing a point-to-point communication between 2 nodes implemented with the LoRa development boards called "mbed" [53] that have external antennas as shown in Figure 3.9, assuring an antenna matched circuitry.

For all the tests, the configuration shown on Table 3.5 was used:

Parameter	Value
Spreading factor (SF)	12
Coding Rate (CR)	4
Bandwidth	500 kHz
Payload	8 bytes

Table 3.5: Configured parameters for LoRa distance test.



Figure 3.9: Test nodes implemented with a MSP430FR5969 LaunchPad Development Kit and the SX1276MB1LAS ARMmbed LoRa board.

First test

In the first test, one of the nodes, configured as receiver, was established on a balcony railing in Montevideo at a height of 4 meters, and the other node, configured as transmitter, was put in a car. Transmitting node continuously sends "hello" word to the receiver every 6 seconds, and the receiver is connected to a PC with a terminal software where received data could be observed. The car was driven in a straight direction until data was lost and no "hello" word was received.

Results are shown in Figure 3.10 and Figure 3.11.



Figure 3.10: Communication distance measured in 3 different directions at the first test.

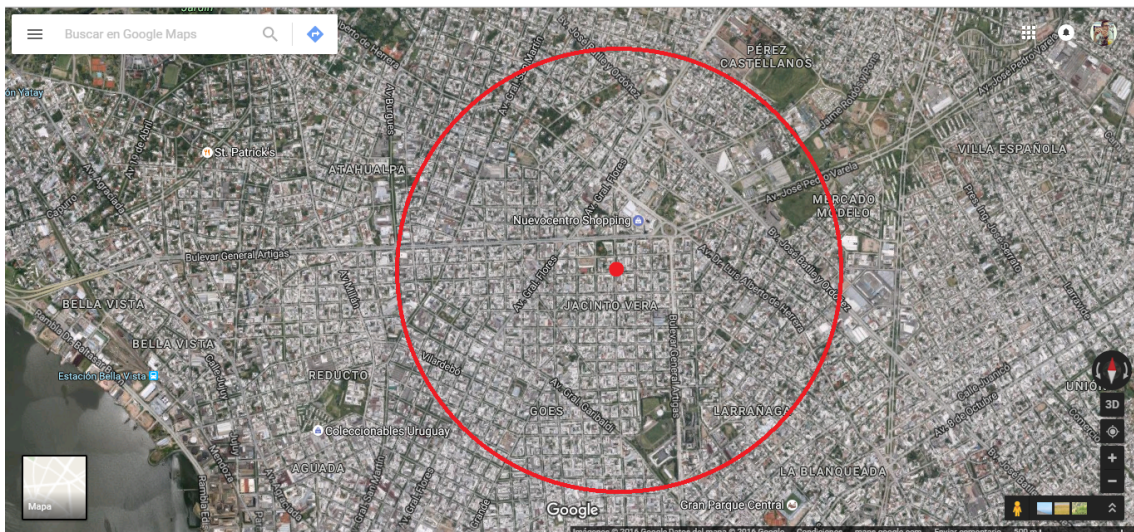


Figure 3.11: Cover area measured in the first test. Radius = 1.38 km. Area = 600 ha approx.

As Semtech states that in the dense city LoRa communication range reaches 2 km between a node and a gateway (the latter hanging a big antenna), the result of 1.4 km was taken as acceptable.

Second test

The second test was developed a few days later at the center of Montevideo. The receiver node was placed on the 25th floor of a centric building ("Torre del Gaucho"), while the transmitter node was put in a car. The test implemented was the same as First test but results are quite different. See Figure 3.12.

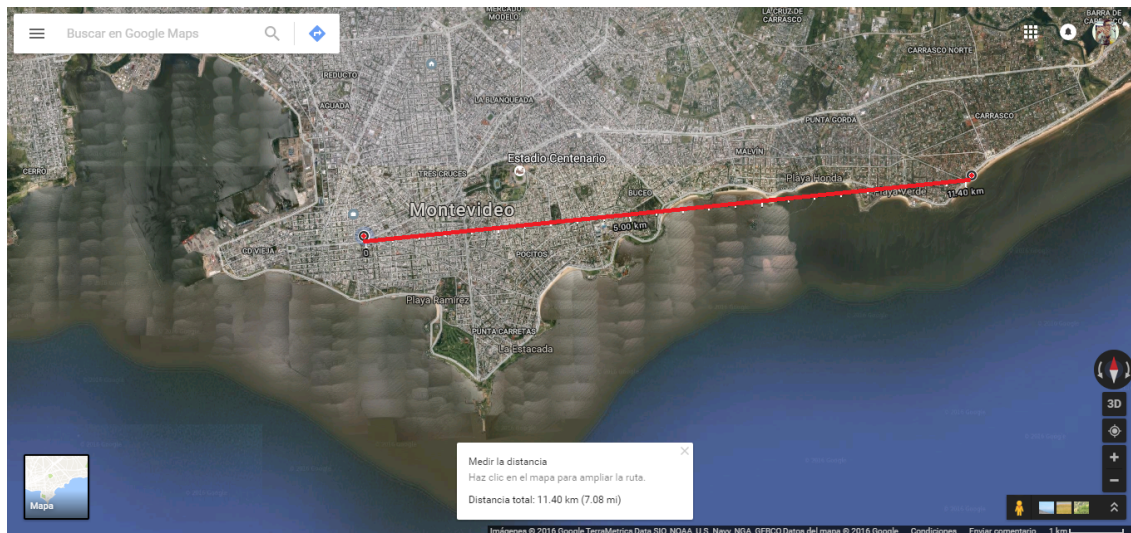


Figure 3.12: Cover area measured in the second test. Distance covered = 11.4 km.

Third test

After LoRa technology communication distance range was successfully verified with the first two tests, the next test to be implemented was to verify communication distance range with the designed platform. To do so, the same test as the first one was done, but instead of the mbed platform as transmitter, the designed board with its **chip antenna** was used.

Although the measured distance range was a bit shorter ($\approx 1km$) than in the first test, it was taken as acceptable, taking in account that the impedance matching circuitry of the antenna is not tuned. It is expected to have a significant improvement in the distance range, reaching 1.2 km - 1.4 km for the same test, with a correct impedance calibration implemented with the process described in 2.1.7.1.

Chapter 4

Conclusions

The design and measurement results of an ultra low power platform including wireless long range communication aimed at collecting activity data for heat detection on cattle was presented. The solution was developed using state of the art of-the-shelf components, reaching very good power consumption and wireless distance range results. The system consumes an average current of only 3 μA while continuously capturing acceleration samples, reaching a typical 5 years battery life for a Polymer Lithium Manganese Dioxide battery of 400 mAh, and transmitting data each hour over 10 km distance to the nearest gateway using the new wireless LoRa technology.

Battery lifetime strongly depends on transmitting time ("time on air" or TOA), which at the same time depends on LoRa parameters configuration. Table 4.1 and Figure 4.1 show battery lifetime variation depending on LoRa parameters: Spreading Factor (SF), Coding Rate (CR), and Bandwidth (BW). Note that for a best and worst case, using a 400 mAh battery, battery lifetime is 2424 days and 383 days respectively. However, according to LoRaWAN specification for US region [39], transmission time must not exceed 400 ms, leading to the parameters combination that are not painted in grey shown at Table 4.1. Without grey rows, battery lifetime is between 2424 days and 1054 days, and a typical value could be taken at a point in the middle of the edges, wherewith battery lifetime could be estimated for 1700 days (almost 5 years) for a continuous use. Battery lifetime could easily be improved even more detecting when the cow is sleeping, putting the accelerometer in its sleep mode and LoRa transceiver not transmitting on these periods.

SF	CR	BW (kHz)	TOA (ms)	Averg. Current (uA)	Battery lifetime (days)
7	1	500	9.02	5.50	2424.0
7	4	500	11.33	5.56	2399.0
12	1	500	247.81	11.43	1166.6
12	4	500	296.96	12.65	1054.1
7	1	250	18.05	5.72	2329.1
7	4	250	22.66	5.84	2283.4
12	1	250	495.62	17.58	758.4
12	4	250	593.92	20.02	666.0
11	1	250	247.81	11.43	1166.6
11	4	250	296.96	12.65	1054.1
7	1	125	36.1	6.17	2160.0
7	4	125	45.31	6.40	2082.8
12	1	125	991.23	29.88	446.2
12	4	125	1187.84	34.76	383.6
11	1	125	495.62	17.58	758.4
11	4	125	593.92	20.02	666.0
10	1	125	247.81	11.43	1166.6
10	4	125	296.96	12.65	1054.1

Table 4.1: Battery lifetime variation due to LoRa parameter changes. Transmission times were extracted from LoRa Calculator tool. Gray coloured rows are excluded in analysis due to bigger times than 400 ms.

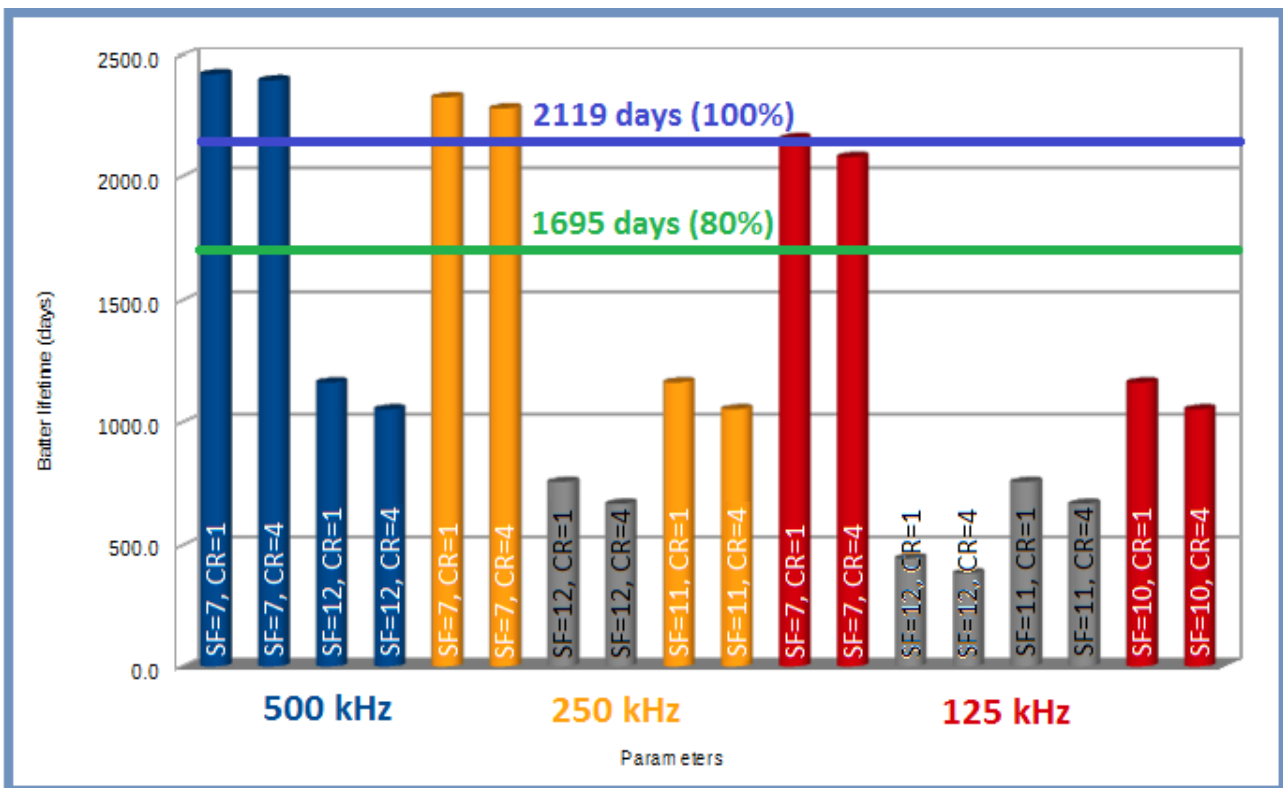


Figure 4.1: Battery lifetime variation due to LoRa parameter changes separated by Bandwidth. Transmission times were extracted from LoRa Calculator tool. A RF switch replacement (Part number: CG2179M2-C4) which has a current consumption of 1 uA was assumed.

The developed platform has the following technical specifications:

- Accelerations range: $\pm 4g$
- Accelerations ODR: 25 Hz
- Output data transmission every hour (configurable).
- Non volatile memory for two hour of data collection.
- Maximum data transmission distance: 11.4 km but still to be determined.
- Current consumption (without wireless transmission): 12 μA (easily reduced to 3 μA).
- Battery: Primary Polymer Lithium Manganese Dioxide battery of 400 mAh.
- Typical battery lifetime: 820 days (2.25 years), but easily improved to a 5 year duration when reducing current consumption from 12 μA to 3 μA .
- Node should be placed on cow's neck one week earlier than heat moment.

To make this device commercial, some improvements and/or fixes should be done first:

- *Plastic case investigation and harsh environment tests:* In order to meet the rough environment requirements, a special plastic case with a belt building a collar should be designed. It must be watertight sealed, preferably IP68 compliant and hardness enough to survive at the harshness of the outdoor countryside.
- *LoRaWAN implementation:* In this work, LoRa physical layer was used and tested, in order to communicate with LoRa gateways, the LoRaWAN protocol should be implemented. When programming LoRaWAN, DIEstro device should act as a Class A device, which are the ones that save more energy and only transmit information periodically.
- *Field tests:* Field tests with hundreds of cows should be done in order to sharpen the detection algorithm after data collection is resolved.
- *LoRa parameters dynamically adjusted:* In order to bring to the LoRa network nodes intelligence, they should be able to determine the best parameters combination to reach the gateway optimizing data transmission time and energy waste. The measure of the RSSI received from the gateway could be used as indicator.
- *Look for a RF switch replacement:* Several RF switches are available at the market with similar characteristics to the used in this project, at a similar price, with current consumption below 5 μA , even there is one with a typical current consumption of 1 μA (Part Number: CG2179M2-C4 from CEL manufacturer).
- *Get some tools and PCB improvements:* Get the proper tool for soldering the accelerometer IC, include test pads, and make some fixes in a new design.

4.1 Improvement opportunities

There are some known improvements which could be done to hit the market with notable differentiations:

- *Geolocation*: It is mentioned on Semtech’s web-page that geolocation can be implemented applying triangulation method with LoRa gateways. It will be of enormous impact in the industry if cattle geolocation can be done without the need of GPS technology.
- *Implement a health status detector*: Based on a rumination recorder, the health status of the cows could be monitored. Bringing the possibility of alert the farmer in case of poor diet, calving moment, disease, etc.
- *Power reduction*: Future work may include further power reductions by means of hardware activity detection modes on the accelerometer, and data processing optimizations.

4.2 Costs and Market

Hardware cost is 25 dollars for 100 units, it will drastically drop for thousands units, and also with time since LoRa and micro-power accelerometer are not yet mature technologies.

Component	Cost (USD)
MSP430FR5969	4.25
SX1276	6.16
ADXL362	7.08
RF Switch	0.54
Crystals	0.94
Battery	1.8
Antenna chip	2.28
Other components	2.80
Total	25.85

Table 4.2: Hardware costs for 100 units production. Based on BOM listed on appendix A.

4.3 Publications

Two different papers are another result of this Master’s degree:

B. Bellini, A. Arnaud, S. Rezk, M. Chiossi: "An Integrated H-Bridge Circuit In A HV Technology". 2016 IEEE 7th Latin American Symposium on Circuits & Systems (LASCAS), pp 331-334, 10.1109/LASCAS.2016.7451077, 2016

This publication is not directly related to the work presented, but it was developed as a final project for the "Introduction to microelectronics" course of the Master’s degree, was presented on LASCAS 2016, which took place at Florianopolis, Brazil. It was selected as one of the papers which have demonstrated the highest quality according to the LASCAS 2016 review process.

B. Bellini, A. Arnaud: ”A 5 μ A Wireless Platform for Cattle Heat Detection”

A paper describing the topic of this documentation was made and submitted to LASCAS 2017.

DIestro is a very interesting, new, and unprecedented technology in the Uruguayan engineering field, which uses state of the art technologies, and that has direct impact to the agribusiness environment, turning this project in one of great potential to the country, to the involved university (Universidad Católica del Uruguay) and to the associate company (BQN). ANII (Agencia Nacional de Investigación e Innovación) observed this potential and supported this project with a scholarship grant.

Bibliography

- [1] Becaluba F., Becaluba H. M.: *Nuevas Tecnologías para el manejo de la detección de celo* at <http://goo.gl/hdq1R8> (December 2016).
- [2] Senger PL.: *The estrus detection problem: new concepts, technologies, and possibilities*. *American Dairy Science Association, J. Dairy Sci.*, Sep. 1994, 77(9):2745-53.
- [3] Vanrell S. R., Chelotti J. O., Galli J. R., Rufiner H. L., Milone D. H.: *3D acceleration for heat detection in dairy cows*. *6o Congreso Argentino de Agroinformática, ISSN 1852-4850, 2014*
- [4] Terreno F., Fernandez J. M., Cattáneo D. S.: *Sistema detector de celo*, *Facultad Regional Villa María de la Universidad Tecnológica Nacional, 2013* at <https://goo.gl/yY6H1E> (December 2016).
- [5] Jonsson R., Blanke M., Poulsen N. K., Caponetti F., Hojsgaard S.: *Oestrus detection in dairy cows from activity and lying data using on-line individual models*. *Elsevier, Computers and Electronics in Agriculture, Dec. 2010, 76(2011)6-15*.
- [6] Firk R., Stamer E., Junge W., Krieter J.: *Automation of oestrus detection in dairy cows: a review*. *Elsevier, Livestock Production Science, 75 (2002) 219-232*
- [7] Bosques-Méndez, J.: *Estrategias de detección de celo para ganado lechero*, *Animal and Dairy Science Department, University of Georgia, July 2013* at <https://goo.gl/xab8ts> (December 2016).
- [8] C. Chen and H. Lin: *Estrus Detection for Dairy Cow Using ZigBee-Based Sensor Networks*. *International Journal of Information and Electronics Engineering, Vol. 5, No. 4, July 2015*.
- [9] D. Hanson, C. Mo: *Monitoring Cattle Motion using 3-axis Acceleration and GPS Data*. *Journal of Research in Agriculture and Animal Science, Volume 2, Issue 10 (2014), pp: 01-08, ISSN(Online) : 2321-9459*.
- [10] A. Valenza, J. O. Giordano, G. Lopes Jr., L. Vincenti, M. C. Amundson, P. M. Fricke: *Assessment of an accelerometer system for detection of estrus and treatment with gonadotropin-releasing hormone at the time of insemination in lactating dairy cows*. *American Dairy Science Association, J. Dairy Sci.*, 2012, 95:7115-7127.
- [11] D. Tsai, C. Huang: *A motion and image analysis method for automatic detection of estrus and mating behavior in cattle*. *Elsevier, Computers and Electronics in Agriculture, Mar. 2014, 104(2014) 25-31*.
- [12] L. Yin, T. Hong, C. Liu: *Estrus Detection in Dairy Cows from Acceleration Data using Self-learning Classification Models*. *Journal of Computers, Vol. 8, No. 10, October 2013*.

- [13] Bikker J. P., van Laar H., Rump P., Doorenbos J., van Meurs K., Griffioen G. M., Dijkstra J.: *Evaluation of an ear-attached movement sensor to record cow feeding behavior and activity. American Dairy Science Association, J. Dairy Sci., Feb. 2014, 97:2974-2979*
- [14] Webpage CowManager: <https://www.cowmanager.com/en-us/> (December 2016)
- [15] Webpage IceRobotics: <http://www.icerobotics.com/products/> (December 2016)
- [16] Dutta R., Smith D., Rawnsley R., Bishop-Hurley G., Hills J.: *Cattle Behaviour Classification using 3-axis Collar Sensor and Multi-Classifer Pattern Recognition. 978-1-4799-0162-3/14 Crown, 2014*
- [17] Chen C., Lin H.: *Estrus Detection for Dairy Cow Using Zigbee-Based Sensor Network. International Journal of Information and Electronics Engineering, Vol. 5, No. 4, 10.7763/IJIEE.2015.V5.539, July 2015*
- [18] Hanson D., Mo C.: *Monitoring Cattle Motion using 3-axis Acceleration and GPS Data. Quest Journal, Journal of Research in Agriculture and Animal Science, Volume 2, Issue 10, pp: 1-8, 2321-9459, 2014*
- [19] Aungier S. P. M., Roche J. F., Sheehy M., Crowe M. A.: *Effects of management and health on the use of activity monitoring for estrus detection in dairy cows. American Dairy Science Association, J. Dairy Sci., Dec. 2011, 95:2452-2466*
- [20] Valenza A., Giordano J. O., Lopes Jr. G., Vicenti L., Amundson M. C., Fricke P. M.: *Assessment of an accelerometer system for detection of estrus and treatment with gonadotropin-releasing hormone at the time of insemination in lactating dairy cows. American Dairy Science Association, J. Dairy Sci., Aug. 2012, 95:7115-7127*
- [21] Chanvallon A., Coyral-Castel S., Gatien J., Lamy J., Ribaud D., Allain C., Clement P., Salvetti P.: *Comparison of three devices for automated detection of estrus in dairy cows. Elsevier, Theriogenology, Jun. 2014, 82(2014)734-741*
- [22] Tsai D., Huang C.: *A motion and image analysis method for automatic detection of estrus and mating behavior in cattle. Elsevier, Computers and Electronics in Agriculture, Mar. 2014, 104(2014)25-31*
- [23] McGowan J. E., Burke C. R., Jago J. G.: *Validation of a technology for objectively measuring behaviour in dairy cows and its application for oestrous detection. Proceedings of the New Zealand Society of Animal Production, Vol. 67, pp 136-142, 2007*
- [24] Michaelis I., Hasenpusch E., Heuwieser W.: *Estrus detection in dairy cattle: Changes after the introduction of an automated activity monitoring system?. Tierärztliche Praxis Großtiere, Issue 3, pp: 159-165, 1434-1220, 2013*
- [25] Silper B. F., Robles I., Madureira A. M. L., Burnett T. A., Reis M. M., de Passille A. M., Rushen j., Cerri R. L. A.: *Automated and visual measurements of estrous behavior and their sources of variation in Holstein heifers. I: Walking activity and behavior frequency. Elsevier, Theriogenology, Dec. 2014, 84(2015)312-320*
- [26] Silper B. F., Polsky L., Luu J., Burnett T. A., Rushen J., de Passille A. M., Cerri R. L. A.: *Automated and visual measurements of estrous behavior and their sources of variation in Holstein heifers. II: Standing and lying patterns. Elsevier, Theriogenology, Dec. 2014, 84(2015)333-341*

- [27] Firk R., Stamer E., Junge W., Krieter J.: *Improving oestrus detection by combination of activity measurements with information about previous oestrus cases*. Elsevier, *Livestock Production Science*, Nov. 2002, 82(2003)97-103
- [28] Rutten C. J., Velthuis A. G. J., Steeneveld W., Hogeveen H.: *Invited review: Sensors to support health management on dairy farms*. American Dairy Science Association, *J. Dairy Sci.*, Dec. 2012, 96:1928-1952.
- [29] Jacobs J. A., Siegford J. M.: *Invited review: The impact of automatic milking systems on dairy cow management, behavior, health, and welfare*. American Dairy Science Association, *J. Dairy Sci.*, 2013, 95:2227-2247.
- [30] Ismael A., Strandberg E., Berglund B., Fogh A., Lovendahl P.: *Seasonality of fertility by physical activity traits in Holstein cows*. American Dairy Science Association, *J. Dairy Sci.*, 2016, 99:1-12.
- [31] Aungier S. P. M., Roche J. F., Duffy P., Scully S., Crowe M. A.: *The relationship between activity clusters detected by an automatic activity monitor and endocrine changes during the peri-estrous period in lactating dairy cows*. American Dairy Science Association, *J. Dairy Sci.*, 2015, 98:1666-1684.
- [32] Webpage Semtech: http://www.semtech.com/wireless-rf/internet-of-things/what_is_lora.html (October 2016)
- [33] Webpage LoRa Alliance: <https://www.lora-alliance.org/> (December 2016)
- [34] STMicroelectronics: *LIS3DH, MEMS digital output motion sensor ultra low-power high performance 3-axes "nano" accelerometer Datasheet, Doc ID 17530, Rev 1, May 2010*.
- [35] Freescale Semiconductor, Inc: *FXLN83xxQ, Xtrinsic FXLN83xxQ 3-Axis LowPower Analog-Output Accelerometer Datasheet, Rev 2.0, July 2014*.
- [36] Analog Devices: *ADXL362 Data Sheet, Rev D, 2015* at <http://goo.gl/8sLMWW> (December 2015)
- [37] LoRa Alliance, Technical Marketing Workgroup: *LoRaWAN, What is it?, A technical overview of LoRa and LoRaWAN, version 1.0, June 2016*.
- [38] Webpage The Things Network: <https://www.thethingsnetwork.org/> (December 2016)
- [39] LoRa Alliance, Inc.: *LoRaWAN Regional Parameters Specification, v1.0, July 2016*.
- [40] Semtech: *LoRa SX1276/77/78/79 Datasheet, Rev. 4, March 2015*
- [41] Texas Instruments: *MSP430FR59xx Mixed-Signal Microcontrollers, Datasheet SLAS704E, October 2012, Revised March 2015*
- [42] Semtech: *LoRaWAN MCU Specification and Requirements. AN1200.28, Rev. 2, July 2015*
- [43] Peregrine Semiconductor: *PE4259 SPDT High Power UltraCMOS 10 MHz-3.0 GHz RF Switch Product Specification, DOC-03694-3, 2016*.
- [44] Hitachi Maxell: *CR2032 - Lithium Manganese Dioxide Battery Datasheet, November 2008*.
- [45] Texas Instruments: *Coin cells and peak current draw. White Paper, SWRA349, 2010*.
- [46] Nordic Semiconductor: *High pulse drain impact on CR2032 coin cell battery capacity. 2011*.
- [47] MinMax Energy Technology Co. Ltd.: *CR024032 - Polymer Li/MnO2 Batteries Specification, October 2016*.

- [48] Texas Instruments: *TPS6274x 360nA IQ Step Down Converter For Low Power Applications Datasheet. SLVSB02B, July 2014.*
- [49] Semtech: *RF Design Guidelines: PCB Layout and Circuit Optimization, Application Note, AN 1200.04, 2006.*
- [50] Semtech: *SX1232 LNA and PA Impedance Matching Techniques, Application Note, AN1200.16, June 2013.*
- [51] Webpage Digilent Electronics Explorer: <https://goo.gl/ruuymI>. (October 2016)
- [52] Webpage Digilent WaveForms: <https://goo.gl/rcV536>. (October 2016)
- [53] Webpage ARMmbed: <https://developer.mbed.org/components/SX1276MB1xAS/> (December 2016)
- [54] Semtech: *SX1272/3/6/7/8: LoRa Modem Designer's Guide. AN1200.13, Rev. 1, July 2013*
- [55] Texas Instruments: *MSP430 FRAM Quality and Reliability, Application Report, SLAA526A, March 2012, Revised May 2014.*
- [56] Texas Instruments: *MSP430 FRAM Technology - How To and Best Practices, Application Note, SLAA628, June 2014*
- [57] Texas Instruments: *Bootloader (BSL) Scripter User's Guide. SLAU655, November 2015.*
- [58] Texas Instruments: *MSP430FR57xx, MSP430FR58xx, MSP430FR59xx, MSP430FR68xx, and MSP430FR69xx Bootloader (BSL) User's Guide. SLAU550E, January 2014, Revised May 2016.*

Appendices

Appendix A

Schematic Circuit and BOM

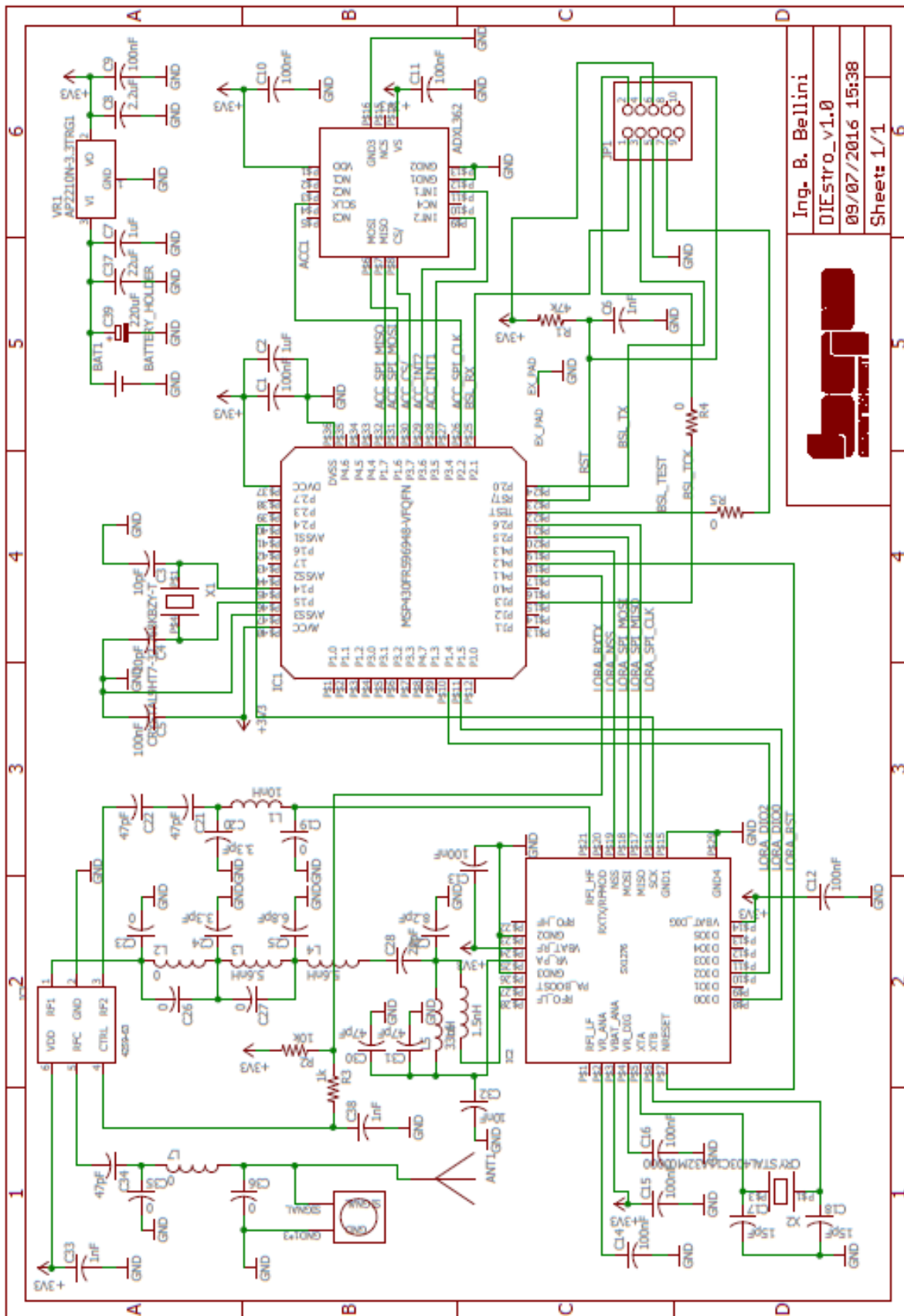


Figure A.1: Schematic circuit for DIEstro project.

Bill of Materials – DIEstro_v1.0							Cost	
Resistors (Ω):	Qty:	Layout Name	Manufacturer Number:	Manufacturer:	Package/Case:	X 100	x1000	
1k	1	R3	RC0603JR-071KL	Yageo	0603	0.0044	0.0027	
10k	1	R2	RC0603JR-0710KL	Yageo	0603	0.0044	0.0027	
47k	1	R1	RC0603FR-0747KL	Yageo	0603	0.0057	0.0035	
Capacitors (F):								
3.3p	2	C20,C24	CL10C3R3CB8NNNC	Samsuung Electro-Mechanics America, Inc.	0603	0.0302	0.0216	
6.8p	1	C25	CL10C8R8CB8NNNC	Samsuung Electro-Mechanics America, Inc.	0603	0.0187	0.0133	
8.2p	1	C29	CL10C8R2CB8NNNC	Samsuung Electro-Mechanics America, Inc.	0603	0.0228	0.0163	
10p	2	C3,C4	C0603C100J5GACTU	Kemet	0603	0.0276	0.0192	
15p	2	C17,C18	CL10C150JB8NNNC	Samsuung Electro-Mechanics America, Inc.	0603	0.0228	0.0163	
22p	1	C28	06035A220JAT2A	AVX Corporation	0603	0.0121	0.0086	
47p	5	C21,C22,C30,C31,C34	CL10C470JB8NCNC	Samsuung Electro-Mechanics America, Inc.	0603	0.056	0.0399	
1n	3	C6,C33,C38	GRM188R71H102KA01D	Murata Electronics North America	0603	0.0273	0.0191	
10n	1	C32	CC0603KRX7R9BB103	Yageo	0603	0.0081	0.0057	
100n	10	C12,C13,C14,C15,C16	CC0603KRX7R7BB104	Yageo	0603	0.085	0.0598	
1u	2	C2,C7	GRM188R61C105KA93D	Murata Electronics North America	0603	0.0308	0.0216	
2.2u	1	C8	GRM188R61C225KE15D	Murata Electronics North America	0603	0.038	0.0268	
22u	1	C37	GRM188R61A226ME15D	Murata Electronics North America	0603	0.1	0.0663	
220u	1	C39	865080143009	Würth Electronics Inc	0603	0.2073	0.1617	
Inductors (H):								
1.5n	1	L6	B82496C3159A	EPCOS	0603	0.2857	0.2505	
5.6n	2	L3,L4	LQW18AN5N6C00D	Murata Electronics North America	0603	0.231	0.198	
10n	1	L1	HK160810NJ-T	Taiyo Yuden	0603	0.0574	0.0492	
33n	1	L5	LQW18AN33NJ00D	Murata Electronics North America	0603	0.105	0.09	
Voltage Regulators:								
2.05V	1	VR1	MCP1703AT-2052E/CB	Microchip Technology	SOT-23-3	0.41	0.41	

Figure A.2: BOM List part 1.

Integrated Circuits:													
MSP430	1	IC1	MSP430FR5968IRGZR	Texas Instruments	48-VQFN	4.2512	3.6167						
SX1276	1	IC2	SX1276IMLTRT	Semtech Corporation	28-VQFN	6.1632	5.136						
ADXL362	1	ACC1	ADXL362BCCZ-RL7	Analog Devices Inc.	16-TFLGA	7.0835	6.1932						
RF_Switch	1	IC3	4259-63	Peregrine Semiconductor	SOT-363	0.53564	0.5356						
Crystals:													
32.768kHz	1	X1	9HT7-32.768KBZY-T	TXC CORPORATION	4-SMD, Flat Leads	0.33	0.3135						
32.000MHz	1	X2	403C11A32M0000	CTS-Frequency Controls	4-SMD, No Lead	0.6061	0.5742						
Other Components:													
Battery Holder	1	BAT1	BU2032SM-BT-GTR	MPD (Memory Protection Devices)	---	0.6609	0.63						
Antenna Connector	1	US12	734120110	Molex, LLC	---	0.5273	0.4585						
Antenna Spring	1	ANT1	ANT-918-HETH	Linx Technologies Inc.	---	0.86	0.86						
Antenna Chip	1	ANT2	ANT1204LL05R0915A	Yageo	---	2.277	1.8454						
PCB	1					0.49	0.284						
Battery 1	1		CR2032	Maxell	---	0.2524	0.2163						
Battery 2	1		CT024032	MinMax	---	1.8	1.5						
Total Bat 1	with	Spring Antenna				US\$ 23.55054	20.321						
Total Bat 1	with	Chip Antenna				US\$ 24.96754	21.306						
Total Bat 2	with	Spring Antenna				US\$ 24.43724	20.975						
Total Bat 2	with	Chip Antenna				US\$ 25.85424	21.96						
Total Mounted	with	Spring Antenna				US\$ 23.69724	20.251						
Total Mounted	with	Chip Antenna				US\$ 25.11424	21.236						

Figure A.3: BOM List part 2.

Appendix B

FW Modules

A detailed description of all the firmware modules implemented is presented in this appendix. Program code is divided into three folders: *app*, *cpu*, and *platform*. Each folder content is detailed below:

app

Contains files and modules related with the application.

- accel
 - ◊ accel.h: defines many values related to the accelerometer, as FIFO's watermark value, sample time, sample size, etc.
- LoRa
 - ◊ lora.h: defines all the LoRa communication customizable parameters as Frequency, Payload size, Spreading factor, Coding rate, etc.
 - ◊ lora.c: implements LoRa transmission function and callbacks functions.
- main.c:

cpu

Contains files and modules related specifically with the used cpu and other general functions.

- clock.h: This file contents all definitions and function headers used for the microcontroller's clock configuration.
- clock.c: This file contents all function implementations used for the microcontroller's clock configuration.
- fram.h: Defines FRAM data partition and sizes for program and user data.
- spi.h: This file contents all definitions and function headers used for controlling and using microcontroller's spi module.

- spi.c: This file contents all function implementations used for controlling and using microcontroller's spi module.
- timeout.h: Defines a timeout_t type and functions headers for timeout functions.
- timeout.c: Implements functions to manage system timeouts based on timers.
- timer.h: Timer configuration definitions.
- timer.c: CPU timers control to generate a time base for the system.
- uart.h: This file contents all definitions and function headers used for controlling and using microcontroller's uart module used for debugging.
- uart.c: This file contents all function implementations used for controlling and using microcontroller's uart module used for debugging.

platform

Contains files and modules related specifically with the designed board and used hardware.

- platformHardwareProfile.h: This file contents all macro definitions for hardware configuration MSP-EXP430FR5969 Launchpad is used.
- adxl362
 - ◊ adxl362.h: Accelerometer's registers definitions and functions headers.
 - ◊ adxl362.c: Accelerometer's control and configuration functions implementation.
- SX1276
 - ◊ enums
 - * enums.h: Enums and data types for controlling the SX1276 transceiver.
 - ◊ radio
 - * radio.h: Radio drivers types and definitions.
 - ◊ registers
 - * sx1276Regs.LoRa.h: SX1276 internal registers addresses for LoRa modem.
 - * sx1276Regs.Fsk.h: SX1276 internal registers addresses for FSK modem.
 - ◊ sx1276
 - * sx1276_hal.h: Generic SX1276 driver definitions and functions headers.
 - * sx1276_hal.c: Generic SX1276 driver implementation.
 - * sx1276.h: SX1276 framework definitions and functions headers.
 - * sx1276.c: SX1276 framework implementation.
 - ◊ typedefs
 - * typedefs.h: Data types definitions for the SX1276 hardware platform.

Appendix C

Long Range Wireless Communication - LoRa

Principles of LoRa Design [54]

LoRa Modulation

LoRa is a **spread spectrum modulation** scheme that uses wideband linear frequency modulated pulses whose frequency increases or decreases over a certain amount of time to encode information. The main advantages of this approach are twofold: a substantial increase in receiver sensitivity due to the processing gain of the spread spectrum technique and a high tolerance to frequency misalignment between receiver and transmitter.

To better understand how to implement a radio design using the LoRa modulation format it is necessary to briefly examine the factors influencing radio receiver sensitivity.

Receiver Sensitivity

The sensitivity of a radio receiver at room temperature is given by:

$$S = -174 + 10\log_{10}BW + NF + SNR \quad (\text{C.1})$$

The first term is due to thermal noise in 1 Hz of bandwidth and can only be influenced by changing the temperature of the receiver. The second term, BW, is the receiver bandwidth. NF is the receiver noise figure and is fixed for a given hardware implementation. Finally, SNR represents the signal to noise ratio required by the underlying modulation scheme. It is **the signal to noise ratio and bandwidth that are available as design variables** to the LoRa designer.

SNR and Spreading Factor

The basic premise of spread spectrum is that each bit of information is encoded as multiple chips. The relationship between the bit and chip rate for LoRa modulation, and respectively, is given by:

$$R_c = 2^{SF} R_b \quad (\text{C.2})$$

where SF is the spreading factor.

SNR Is the minimum ratio of wanted signal power to noise that can be demodulated. The performance of the LoRa modulation itself, forward error correction (FEC) techniques and the spread spectrum processing gain combine to allow significant SNR improvements. Some example SNRs for both conventional GMSK¹ and LoRa modulation formats are shown in the table below. The lower this number the more sensitive the receiver will be. Negative numbers indicate the ability to receive signal powers below the receiver noise floor:

Modulation	Typical SNR
LoRa SF12	-20 dB
LoRa SF10	-15 dB
GMSK	9 dB

Table C.1: SNR for Various Modulation Configurations

The substitution of one bit for multiple chips of information means that the spreading factor has a direct influence on the duration of the LoRa packet. The influence of the spreading factor on the sensitivity and the time on air are shown below for a fixed bandwidth of 250 kHz.

SF	Time on air [ms]	Sensitivity [dBm]
12	528.4	-134
10	132.1	-129
8	39.2	-124

Table C.2: Influence of SF on Time on Air and Sensitivity (CR=2, BW=250)

BW and Chip Rate

One of the principle design compromises that the designer must manage in the selection of spreading factor is that of time on air (packet duration) versus occupied bandwidth. The representation of a single bit by many chips, implies that the chips must either be sent faster than the original bitrate - increasing the occupied bandwidth of the signal, or in the same bandwidth - increasing the time taken to transmit the information.

LoRa modulation sends the spread data stream at a chip rate equal to the programmed bandwidth in chips-per-second-per-Hertz. So a LoRa bandwidth of 125 kHz corresponds to a chip rate of 125 kcps.

Equation C.1 shows that an increase in bandwidth (BW) due to the integration of additional noise power in the channel, will desensitize the receiver. Meaning that for a given spreading factor the designer can either elect to use a narrow bandwidth, maximizing sensitivity but increasing time on air or increasing the bandwidth for faster transmission but reducing sensitivity.

Figure C.1 shows the example of the SX1272, which has three programmable bandwidth settings 500 kHz, 250 kHz and 125 kHz (as shown below). (The SX1276 has bandwidths from 500 kHz to as low as 7.8 kHz).

¹Gaussian Minimum Shift Keying

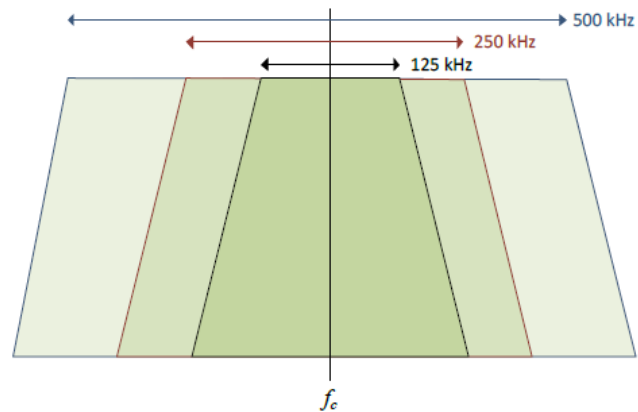


Figure C.1: The LoRa Bandwidth Corresponds to the Double Sided Transmit Spectrum Bandwidth.

For a fixed spreading factor the influence of bandwidth on the resulting time on air and sensitivity are shown in the table below for a 10 byte payload packet:

BW	Time on air [ms]	Sensitivity [dBm]
125	264.2	-132
250	132.1	-129
500	66	-126

Table C.3: Influence of BW on Time on Air and Sensitivity (CR=2, SF=10)

Examination of the basic design criterion of bandwidth and spreading factor allow quick evaluation of the suitability of LoRa for a given application. However, to optimize design performance there are other design criteria that must also be considered.

Advanced LoRa Design Parameters

In addition to the use of spreading factor and bandwidth there are other design variables that the designer must consider when implementing a LoRa radio link. These are of particular importance when optimizing the robustness to interference and time on air of the LoRa transmission.

Forward Error Correction

The LoRa modem also employs a form of Forward Error Correction (FEC) that permits the recovery of bits of information due to corruption by interference. This requires a small overhead of additional encoding of the data in the transmitted packet. Depending upon the coding rate selected, the additional robustness attained in the presence of thermal noise alone is shown in Figure C.2.

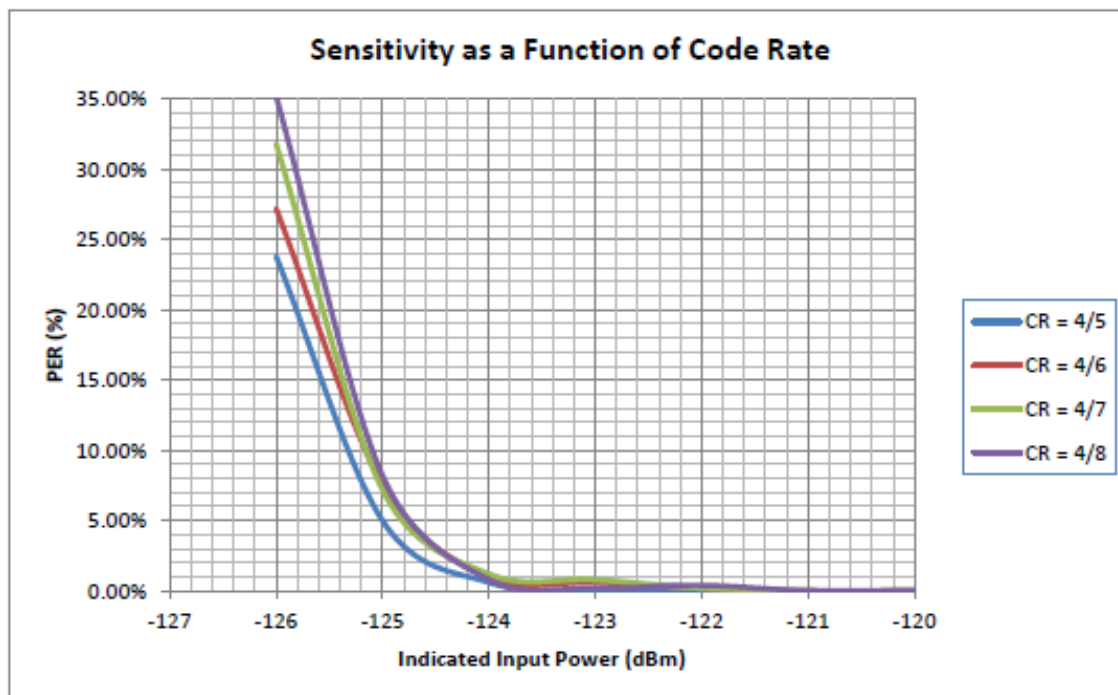


Figure C.2: Influence of Coding Rate on Sensitivity (SF = 7, BW = 125 kHz, 13 Byte Payload).

The real performance gain of FEC, however, is in the presence of bursts of interference. If the radio link is likely to be subject to such interference, the use of FEC should be evaluated.

Table C.4 shows how the increase in coding rate influences time on air for a fixed bandwidth of 250 kHz at SF = 10.

CR	Time on air [ms]
1	123.9
2	132.1
4	148.5

Table C.4: Influence of CR on Time on Air (SF=10, BW=250 kHz)

Hardware Implementation

The receiver RF connection method will further influence the receiver sensitivity and the header mode has an impact on the time on air.

Two receiver input connection, RFI, configurations are possible with the SX1272/3/3/6/7/8. Figure C.3 shows both configurations. Optimal sensitivity performance (by reduction of noise figure, NF, of Equation C.2) is possible by employing individual RF and Tx paths, using separate antennas or an RF switch for single antenna operation.



Figure C.3: Individual RF transmit and receive paths (left) provides better sensitivity than the single shared TRx path (right).

Low Data Rate Optimization Mode & Header Mode

The final two factors that influence the time on air of the packet are two operational modes connected to the modem and packet settings of the modem. To understand their influence it is necessary to examine the format of the LoRa packet.

The LoRa Packet Format & Time On Air

To effectively manage the regulatory and system level design constraints of time on air and receiver sensitivity, it is hence necessary to be able to calculate the time on air of a given modem configuration. The precise formulas are given below.

For calculation of the time on air it is convenient to define symbol duration, T_{sym} . This is the time taken to send 2^{SF} chips at the chip rate so, recalling that the bandwidth defines the chip rate, it is given by:

$$T_{sym} = \frac{2^{SF}}{BW} \quad (C.3)$$

The packet comprises several elements, as shown in Figure C.4.

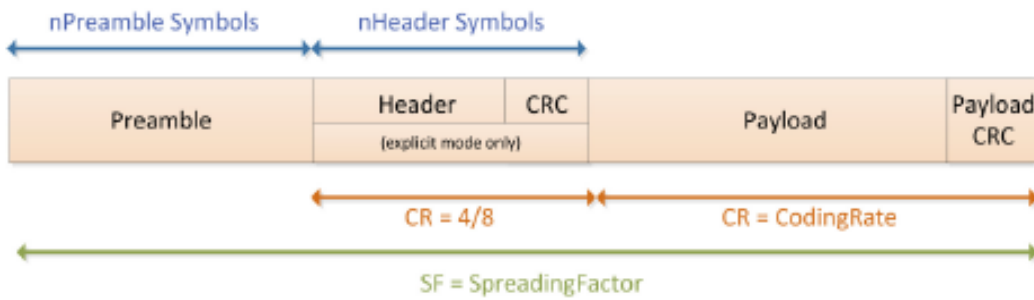


Figure C.4: LoRa Modem Packet formatting.

Common to all modem configurations is a sequence of preamble, whose duration is given by:

$$T_{preamble} = (n_{preamble} + 4.25) T_{sym} \quad (C.4)$$

Where $n_{preamble}$ is the number of programmed preamble symbols. The number of symbols that make up the packet payload and header is given by:

$$payloadSymbNb = 8 + \max \left(\text{ceil} \left(\frac{8PL - 4SF + 28 + 16 - 20H}{4(SF - 2DE)} \right) (CR + 4), 0 \right) \quad (C.5)$$

With the following dependencies:

- PL Is the number of payload bytes.
- SF The spreading factor
- H = 0 when the header is enabled and H = 1 when no header is present.
- DE = 1 when the low data rate optimization is enabled , DE = 0 for disabled.
- CR is the coding rate from 1 to 4

It follows that if the time on air requires reduction, and the packet length is known in advance, then the header information can be removed. The payload duration is then the symbol period multiplied by the number of payload symbols.

$$T_{payload} = payloadSymbNb T_{sym} \quad (C.6)$$

The time on air, or packet duration, is simply then the sum of the preamble and payload duration:

$$T_{packet} = T_{preamble} + T_{payload} \quad (C.7)$$

Here we can see that, in the narrow band regime, the LoRa packet can have a significant duration. To avoid issues surrounding drift of the crystal reference oscillator due to either temperature change or motion, the low data rate optimization bit is used. Specifically for 125 kHz bandwidth and SF = 11 and 12, this adds a small overhead to increase robustness to reference frequency variations over the timescale of the LoRa packet.

LoRa Calculator

In order to simplify design decisions using the LoRa modem there is a software planning tool that allows the quick evaluation of the LoRa modem configuration and the resulting time on air and sensitivity performance. This can be downloaded from www.semtech.com.

Figure C.5 shows the main display of the LoRa calculator. All the design variables can be modified and the resultant RF and time on air performances are calculated without the need to manually calculate the quantities of the design equations.

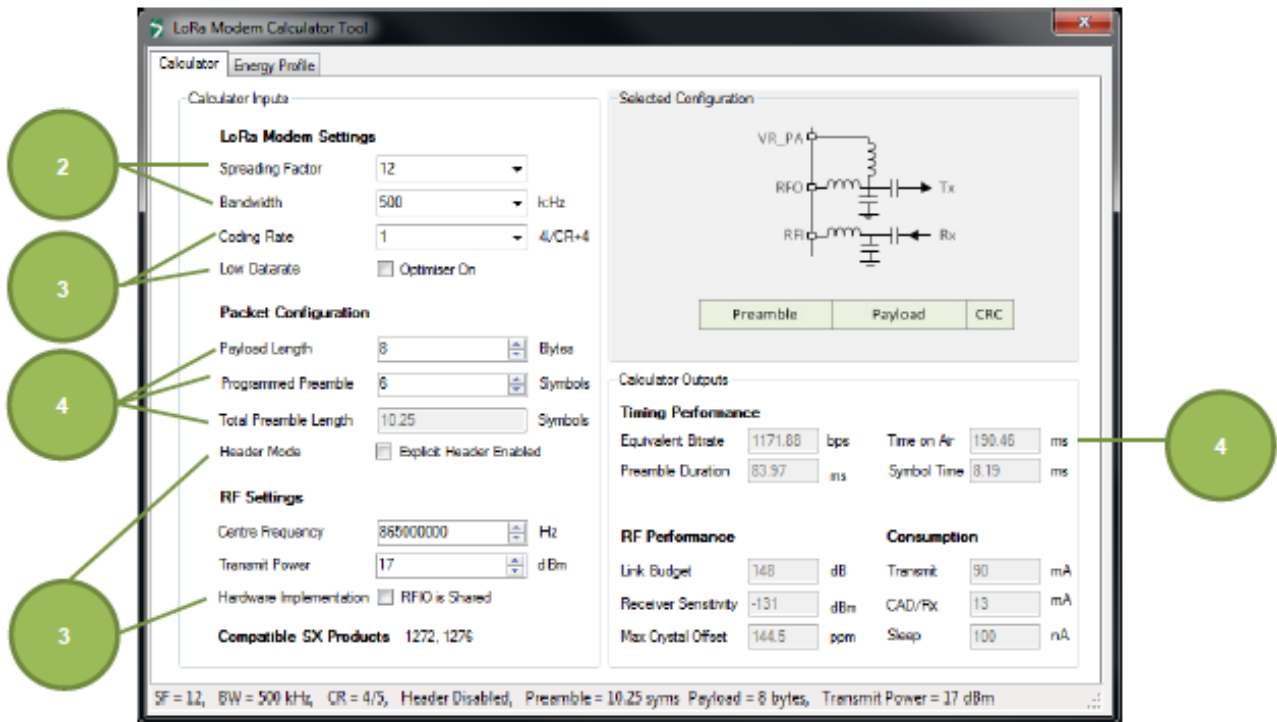


Figure C.5: The LoRa Calculator Interface.

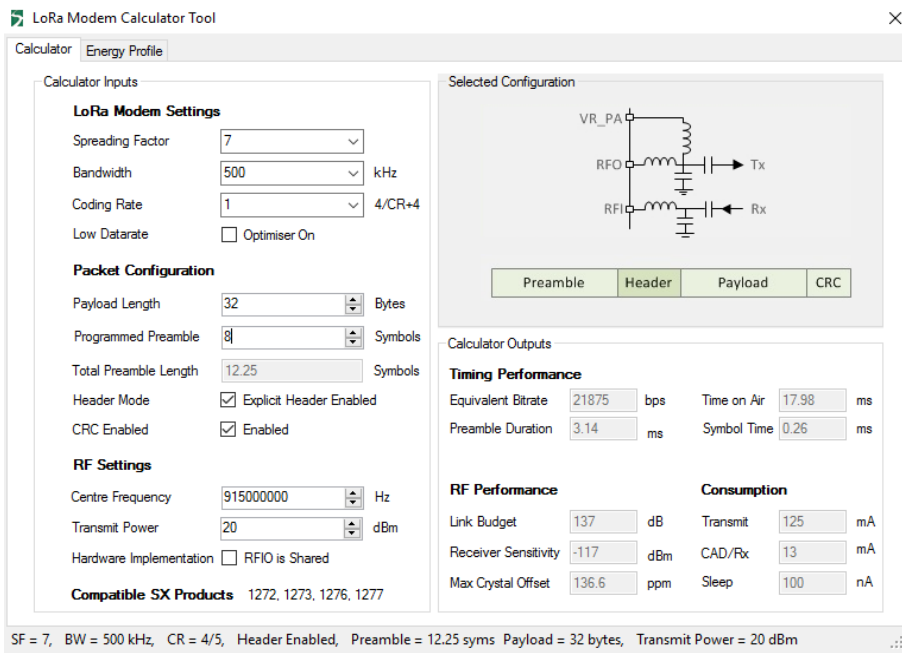


Figure C.6: LoRa Calculator for SF=7, CR=1, PYLD=32.

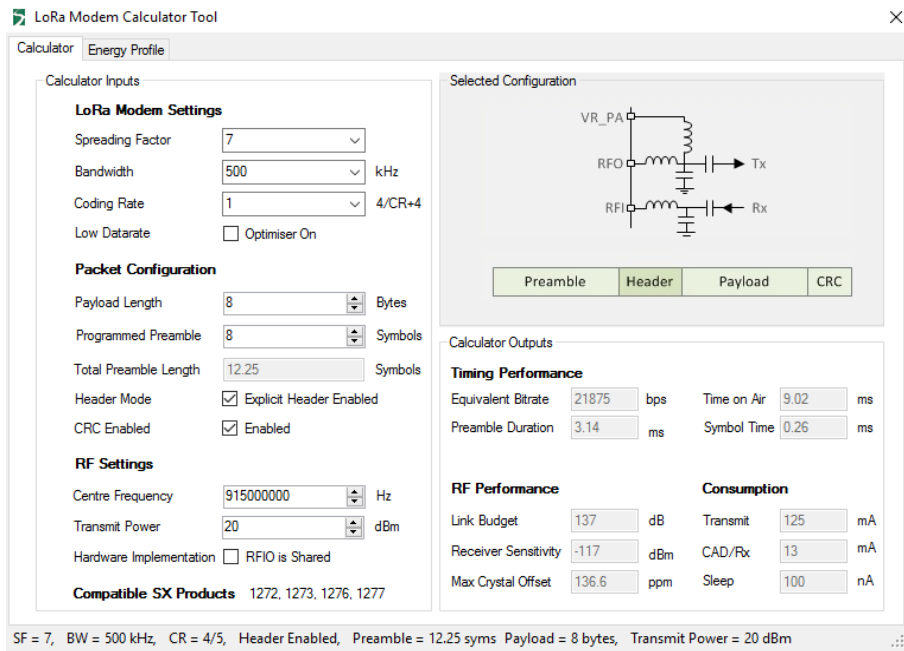


Figure C.7: LoRa Calculator for SF=7, CR=1, PYLD=8.

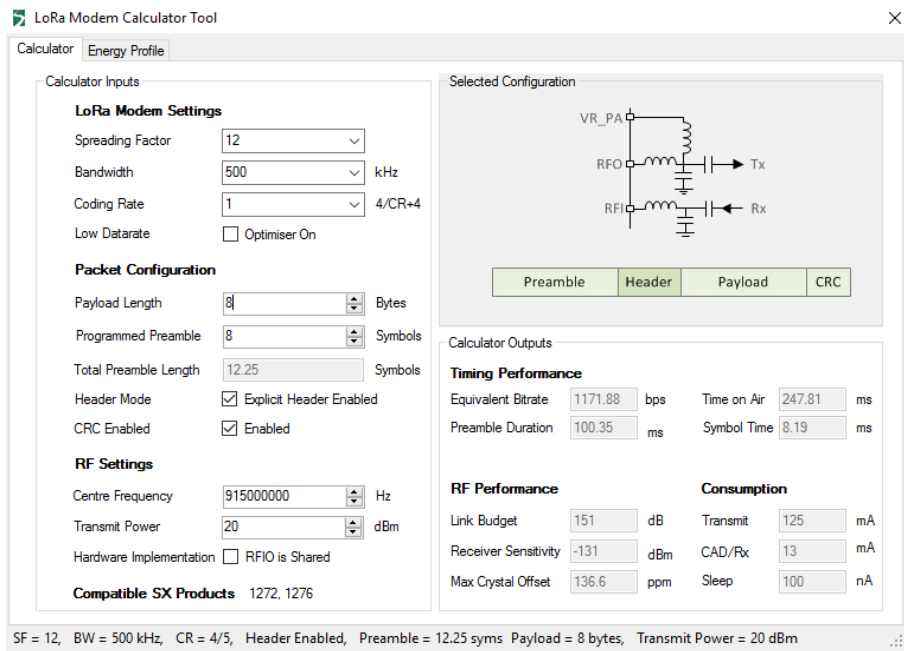


Figure C.8: LoRa Calculator for SF=12, CR=1, PYLD=8.

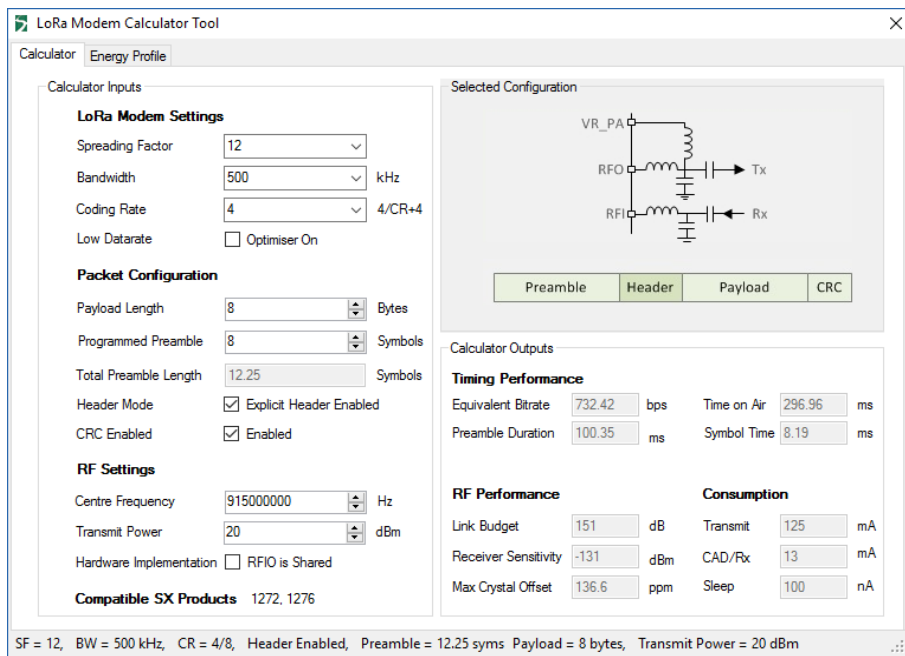


Figure C.9: LoRa Calculator for SF=12, CR=4, PYLD=8.

Appendix D

FRAM

FRAM Technology

Ferroelectric Random Access Memory (FRAM) is an ultra-low power nonvolatile memory technology with write speeds similar to static RAM (SRAM). The technology has been in the industry for over a decade, implemented as stand-alone memory.

Some of the key attributes of FRAM are:[55]

- FRAM is nonvolatile; that is, it retains its contents on loss of power.
- FRAM is a true random-access memory. The memory is not segmented; addressing of data for read or write at word or byte level happens directly in the same way as SRAM.
- The embedded FRAM on MSP430 devices can be accessed (read or write) at a maximum speed of 8 MHz. Above 8 MHz, wait states are used when accessing FRAM. Typical write speeds can exceed 2 MBps with FRAM compared to approximately 14 kBps on flash devices.
- Writing to FRAM and reading from FRAM require no setup or preparation such as pre-erase before write or unlocking of control registers.
- FRAM write accesses are extremely low power, because writing to FRAM does not require a charge pump.
- FRAM writes can be performed across the full voltage range of the device.
- FRAM meets and exceeds reliability requirements on data integrity. It provides practically unlimited endurance for read and write operations on the order of 10^{15} write or erase cycles.

FRAM is a non-volatile memory technology that is very flexible and can be used for program or data memory. It can be written to in a bit-wise fashion and with virtually unlimited write cycles. FRAM does not require a pre-erase in which every write to FRAM is non-volatile. However, there are some minor trade-offs in using FRAM instead of RAM that may apply to a subset of use cases. One of the differences on the MSP430 platform is the FRAM access speed, which is limited to 8 MHz, whereas, SRAM can be accessed at the maximum device operating frequency. Wait-states are required if the CPU accesses the FRAM at speeds faster than 8 MHz. Another trade-off is that FRAM access results in a somewhat higher power consumption compared with SRAM.

Since FRAM memory can be used as universal memory for program code, variables, constants, stacks, and so forth, the memory has to be partitioned for the application. Code Composer Studio IDE can be used to set up an application's memory layout to make best-possible use of the underlying FRAM depending on the application needs. These memory partitioning schemes are located inside the IDE-specific linker command file. By default, the linker command files will typically allocate variables and stacks into SRAM. And, program code and constants are allocated in FRAM. These memory partitions can be moved or sized depending on your application needs.

FRAM Layout Design

[56] In order to have persistent data located in FRAM, but treated as RAM data, several modifications should be done to the linker file and the MPU (Memory Protection Unit) configuration.

Linker changes

In Code Composer Studio, there are two C language pragma statements that can be used: `#pragma PERSISTENT` and `#pragma NOINIT`. `PERSISTENT` causes variables to not get initialized by the C startup routine, but rather the debug tool chain initializes them for the first time as the application code is loaded onto the target device. Subsequently, those variables do not get initialized, for example, after a power cycle as they have been completely excluded from the C startup initialization process. Declaring variables as `PERSISTENT` causes them to get allocated into the `.TI.persistent` linker memory segment.

Here is a code example showing how the variable is declared as persistent:

```
#pragma PERSISTENT(x)
unsigned int x = 5;
```

At the linker file, the new section for DATA in FRAM should be created. In order to achieve this, the following changes were made:

```
GROUP(READ_WRITE_MEMORY)
{\right\rfloor
    /*.TI.persistent : {}*/           /* For #pragma persistent */
    .cio          : {}                /* C I/O Buffer */
    .systemem    : {}                /* Dynamic memory allocation area */
//} PALIGN(0x0400), RUN_END(fram_rx_start) > 0x4400
} PALIGN(0x0400) > DATA_FRAM, RUN_START(fram_rw_start) RUN_START(fram_rx_end)

.TI.persistent : {} >> DATA_FRAM /* For #pragma persistent */
```

MPU changes

Since data is written to a section of FRAM, care must be taken in order not to write code sections. To configure which sections of memory will be write protected it is necessary to do the following steps:

1. Go to Project Properties.

2. On General, move to the MSP430 MPU tab.
3. Select "Enable Memory Protection Unit (MPU)" and select "Manually specify memory segment boundaries and access rights".
4. Set Boundary 1 to 0x4C00 and Read and Execute access rights to Code Segment (Segment 1).
5. Set Boundary 2 to 0xFC00 and Read and Write access rights to Data Segment (Segment 2).
6. Set Read and Execute access rights to Code Segment (Segment 3).
7. Press OK.

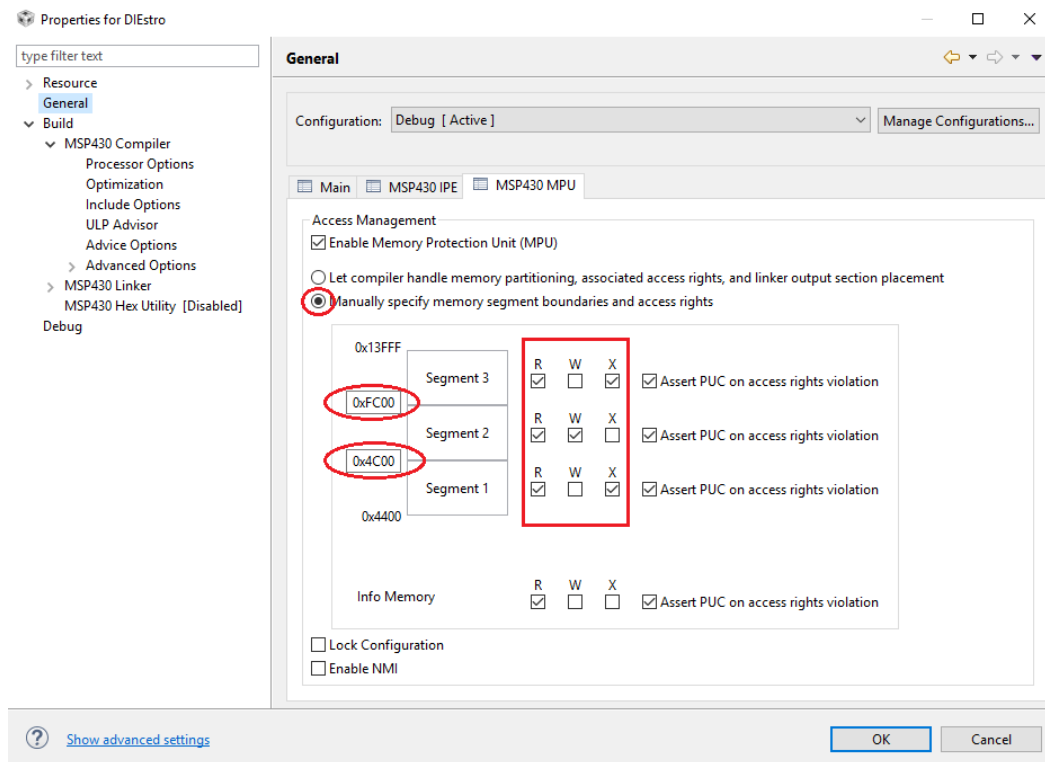


Figure D.1: MPU Configuration window of Code Composer Studio.

Appendix E

BSL-Rocket and BSL-scripter

MSP430-BSL or BSL-Rocket is a joint project between Olimex LTD and Texas Instruments aiming to provide an affordable programmer for MSP430 boards that have embedded Bootstrap loader. The main features of the product are the tiny size and the low price. Other features are listed below:

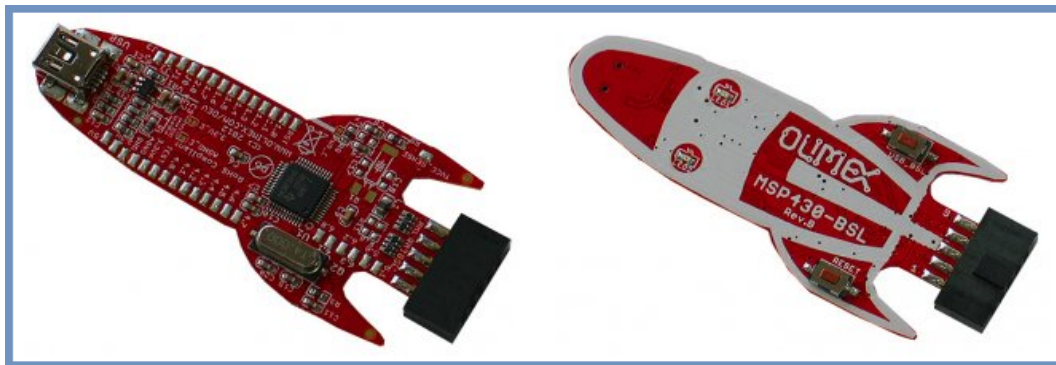


Figure E.1: BSL-Rocket programmer from both sides.

- Ready-to-work with MSP430 microcontrollers with BSL interface.
- Uses TI standard 2x5 pin BSL connector.
- Mini USB compatible with widely used cables from customer devices.
- Can supply target with 150 mA at 3.3 V.
- All free processor pins are available at two rows of pads for custom firmware.
- Two LEDs, available as GPIOs.
- Two buttons, for easier reset and bootloader mode, not available as GPIOs.
- Open hardware board, board schematic and layout available for Eagle.
- Dimensions - (77.5 x 33.0)mm.

The microcontroller has a 2-kilobyte memory section of read only memory (ROM) that can not be customized. The BSL is located between addresses 0x1000 and 0x17FF.

After compiling, Code Composer Studio generate a .txt file which its content is in Intel's hex file format, and this .txt file is the one to be loaded to the MSP430 FRAM memory. In order to do so, the BSL Scripter software should be used.

The BSL Scripter is a PC application that is available for Windows, Linux and Mac OS X. It is a user interface which allows to easily communicate with the BSL on MSP430 and MSP432 devices to modify the device's memory via UART, I2C, SPI or USB. Supported programming adapters are the MSP-BSL programmer and the MSP-FET.

```

C:\windows\system32\cmd.exe
c:\ti\frxx_uart>BSL-Scripter.exe script.txt
-----
BSL Scripter 3.1.0.0
PC software for BSL programming
2015-Nov-18 17:03:57
-----
Input file script is : c:/ti/frxx_uart/script.txt
-----
//
// script.txt
//
MODE FRxx UART COM19
//
MASS_ERASE
  Mass erase done.
//
RX_PASSWORD bsl_passwordFRxx_default.txt
  Read Txt File : c:/ti/frxx_uart/bsl_passwordFRxx_default.txt
  Password is correct.
//
TX_BSL_VERSION
  BSL Version is : BSL_Uendor[00],CI[07],API[34],PI[b2]
//
RX_DATA_BLOCK BlinkLEDfr.txt
  Read Txt File : c:/ti/frxx_uart/BlinkLEDfr.txt
  Time elapsed of writing 256 bytes : 0.3525 seconds
  Speed of writing data :0.7092(kB/s)
  Data received by BSL.
//
SET_PC 0x8000
  Set PC is sent.
c:\ti\frxx_uart>

```

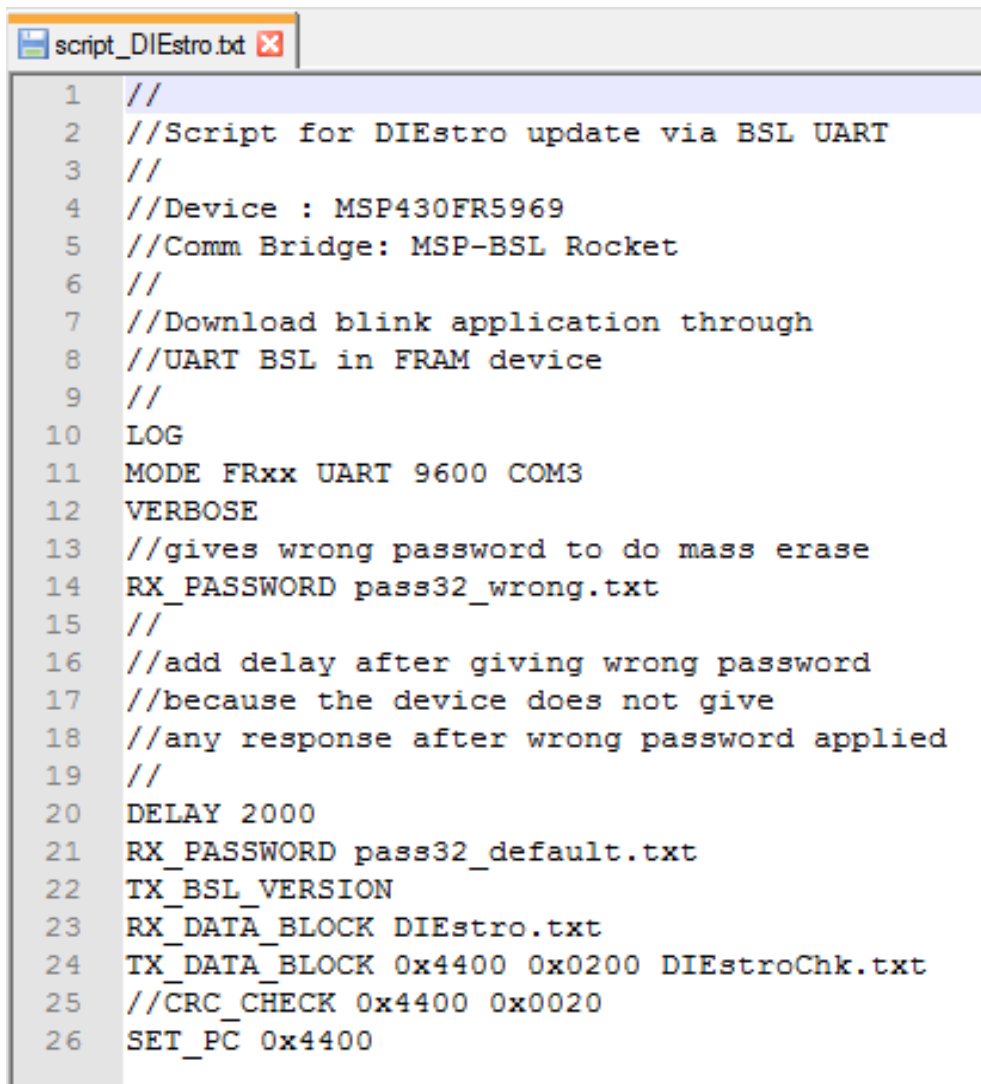
Figure E.2: Bootloader BSL scripiter tool.

BSL scripiter is executed from line command prompt (for Windows OS: bsl-scripiter-windows.exe). After executing, it asks for a script file to run. [57] defines and describes scripts format and programming language. The script file is a ASCII text file. The BSL Scripiter reads this text file to parse the BSL commands. Each line must contain a single BSL command with no preceding spaces. Empty lines are allowed. Some commands may have optional parameters and some may have mandatory parameters.

Figure E.3 shows the implemented script to upload the microcontrollers firmware. The upload sequence implemented by the script is detailed below:

- Enable log information into a .txt file
- Open UART interface at 9600 bps.
- Make verbose to see what is happening at every moment.
- Give a wrong bootloader password to the microcontroller to force mass erase.
- Wait for 2 seconds.
- Give the correct bootloader password to unlock the BSL protected commands if the password matches the top 16 words in the BSL interrupt vector table (located between addresses 0xFFE0 and 0xFFFF).

- Take data from the generated file at compilation stage and program it.
- Read programmed data and store it in a newfile in order to verify programming.
- Set Program Counter to the start of the application.



```
1 //
2 //Script for DIEstro update via BSL UART
3 //
4 //Device : MSP430FR5969
5 //Comm Bridge: MSP-BSL Rocket
6 //
7 //Download blink application through
8 //UART BSL in FRAM device
9 //
10 LOG
11 MODE FRxx UART 9600 COM3
12 VERBOSE
13 //gives wrong password to do mass erase
14 RX_PASSWORD pass32_wrong.txt
15 //
16 //add delay after giving wrong password
17 //because the device does not give
18 //any response after wrong password applied
19 //
20 DELAY 2000
21 RX_PASSWORD pass32_default.txt
22 TX_BSL_VERSION
23 RX_DATA_BLOCK DIEstro.txt
24 TX_DATA_BLOCK 0x4400 0x0200 DIEstroChk.txt
25 //CRC_CHECK 0x4400 0x0020
26 SET_PC 0x4400
```

Figure E.3: Implemented script for BSL scripiter firmware update application.

Appendix F

Previous work

Previous work

At the beginning of this Master's degree project the subject of study was not enough defined and it was to design and develop wireless sensors for the agroindustry. One possible project was to implement temperature and/or humidity sensors for pastures, silo bags, etc. and transmit their information by Near Field Communication (NFC) arising technology, thus the farmers could get sensors information (pastures status) with any smartphone having NFC hardware.

Investigation on PTC and NTC thermistors, microcontrollers, NFC antenna design, and NFC protocol and standards (as ISO 14443, ISO 15693, ISO 18092, among others) was made. Also the M24LR64-R IC, a dynamic NFC/RFID tag IC with 64-Kbit EEPROM with I^2C bus and ISO 15693 RF interface, from STMicroelectronics, was studied.

A simple design where a PIC12 microcontroller uses an ADC to get the NTC thermistor's voltage variation due to temperature changes, and then stores and sends its value through the M24LR64-R IC to a mobile phone, was made.

Figure F.1, F.2, and F.3 shows the schematic circuit, 2 layers pcb design and BOM list, for the described sensor.

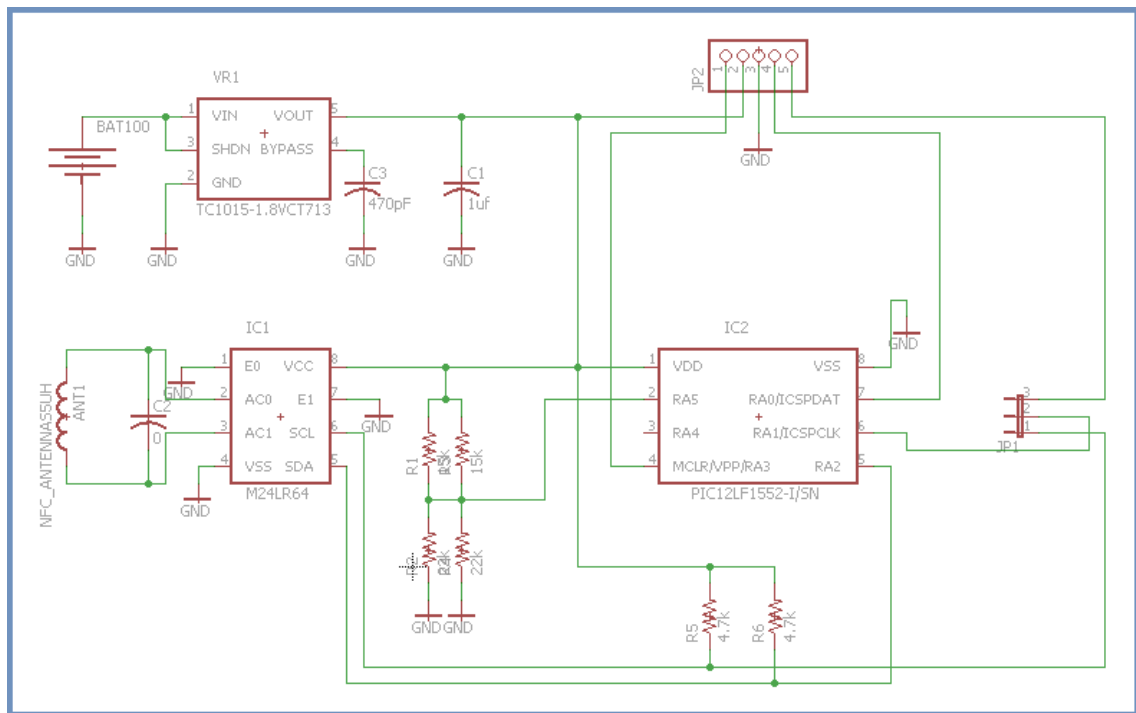


Figure F.1: NFC temperature sensor schematic circuit.

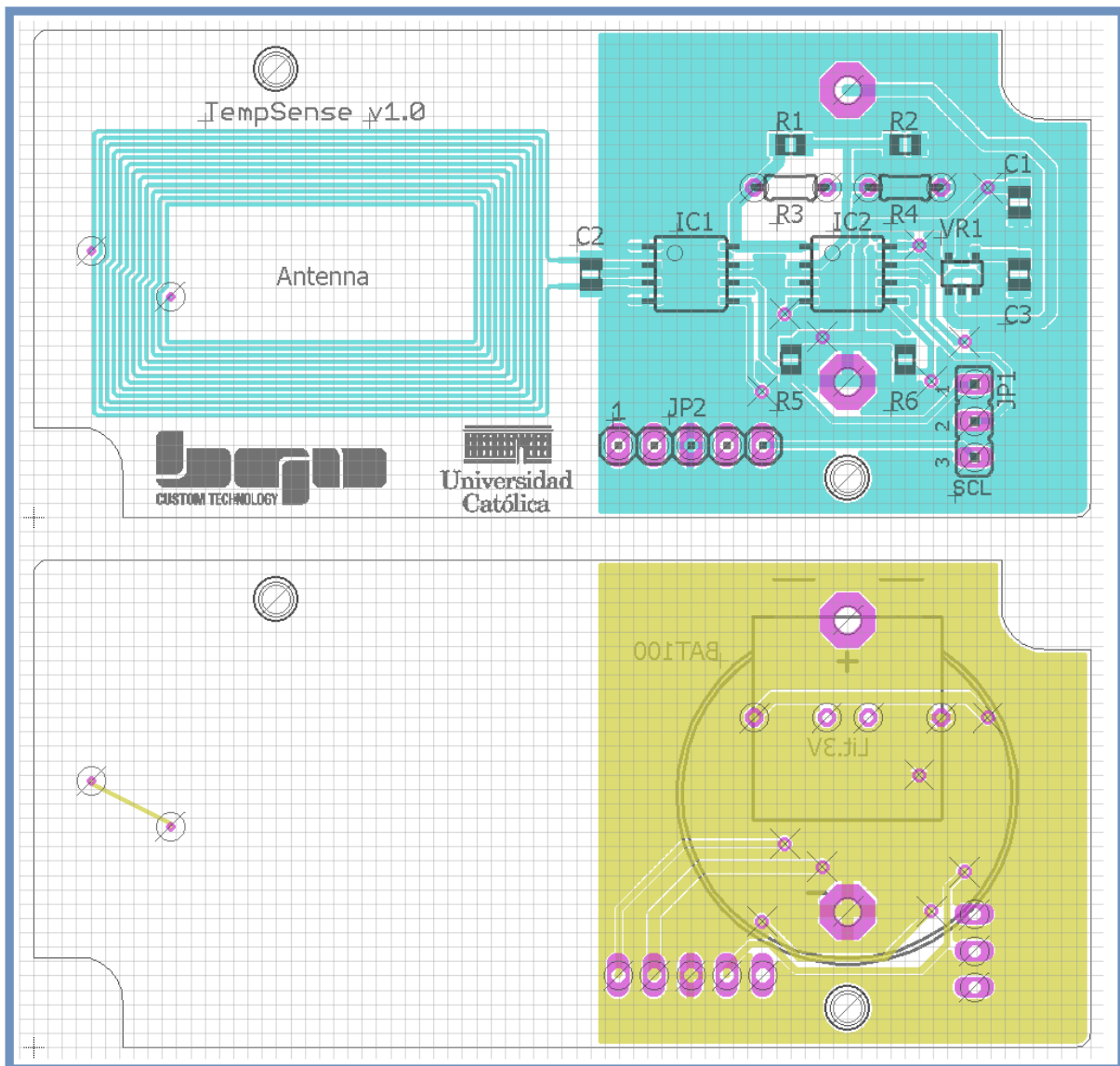


Figure F.2: NFC temperature sensor 2 layer PCB design.

Bill of Materials TempSense_v1.0						
	Qty:	Layout Name:	Manufacturer No:	Manufacturer:	Package/Case:	Mounting:
Resistors (Ω):						
4.7k	2	R5, R6	ERJ-6GEYJ47ZV	Panasonic Electronic Components	0805	SMD
15k	1	R1	RMCF0805FT15K0	Stackpole Electronics Inc	0805	SMD
15k	1	R3	MFR-25BFB52-15K	Yageo	Axial	TH
Capacitors (F):						
470p	1	C3	CL21B471KBANNNC	Samsung Electro-Mechanics America, Inc	0805	SMD
1u	1	C1	CL21B105KPFNNNE	Samsung Electro-Mechanics America, Inc	0805	SMD
Thermistors (Ω):						
22k	1	R4	NTCLE100E3223JB0	Vishay BC Components	Bead	TH
22k	1	R2	NCP21XW223J03RA	Murata Electronics North America	0805	SMD
Voltage Regulators:						
1.8V	1	VR1	TC1015-1.8VCTT713	Microchip Technology	SOT-23-5	SMD
Integrated Circuits:						
M24LR64	1	IC1	M24LR64-RMN6T/2	STMicroelectronics	8-SOIC	SMD
PIC12LF1552	1	IC2	PIC12LF1552-I/SN	Microchip Technology	8-SOIC	SMD
Other:						
Pin Header	1	JP1	M20-9990346	Harwin Inc	---	TH
Battery	1	BAT1	CR2032TH2035	MinMax	2032	TH
Case	1	---	1551KGY	Hammond Manufacturing	---	---
Jumper	1	---	969102-0000-DA	3M	---	---

Figure F.3: NFC temperature sensor BOM list.